Rice Glycoprotein α-Amylase Targeting to Plastid from the Golgi apparatus through the Secretory Pathway

イネ糖タンパク質 α-アミラーゼは
分泌経路とゴルジ体を経由してプラスチド局在化する

Aya Kitajima-Koga

Doctoral Program in Life and Food Sciences
Graduate School of Science and Technology
Niigata University

Contents

Abbreviations

ARF1	ADP-ribosylation factor 1
CAH1	*Arabidopsis* carbonic anhydrase 1
CLSM	confocal laser scanning microscope
COP I, COP II	coat protein complex I, II
DsRed	red fluorescence protein from *Discosoma sp.*
ER	endoplasmic reticulum
EM	electron microscome
GFP	green fluorescent protein
Hip	Hsp70-interacting protein
Hop	Hsp70-organizing protein
Hsp	heat shock protein
mRFP	monomeric red fluorescent protein
ST	transmembrane domain of sialyltransferase
SP	ER signal peptide
SPP	stromal processing peptidase
TEM	transmission electron microscope
Tic	translocon at the inner envelope of chloroplast
Toc	translocon at the outer envelope of chloroplast
TP	transit peptide
TRP	tetratricopeptide repeat
NPP1	rice nucleotide pyrophosphatase/phosphodiesterase 1
WxTP	transit peptide of the rice waxy protein

INTRODUCTION

Cereal α-amylases (EC 3.2.1.1) are typical secretory proteins found in many plants. In germinating cereal seeds, the enzyme molecules are biosynthesized and secreted from the secretory tissues, scutellar epithelium and aleurone, to the starchy endosperm that has programmatically died. Numerous α-amylase isoforms have been identified in cereals, but the predominant α-amylase isoform I-1 (AmyI-1) in rice is a unique glycoprotein that bears *N*-linked oligosaccharide side chains (Hayashi et al., 1990; Terashima et al., 1994). The biosynthesis and secretion of AmyI-1 have been extensively investigated: mRNA translation on endoplasmic reticulum (ER)-membrane-bound ribosomes, signal-sequence-dependent translocation of the ER, core glycosylation in the ER lumen, vesicular transport to the Golgi apparatus, oligosaccharide modification to the complex type, and exocytosis, all proceed according to the canonical secretory mechanism (Palade et al., 1975; Blobel et al., 1980; Kornfeld and Kornfeld, 1985).

Protein targeting into plastids is an essential cellular event for expressing plant function and maintaining plant life. Plastids, including chloroplasts in green leaves and amyloplasts in starchy cells, contain the genetic machinery required to synthesize their own proteins, although most plastidial proteins are encoded in the nuclear DNA. Nuclear-encoded plastidial proteins are normally synthesized in the cytosol and post-translationally imported into the organelle. In most cases, precursor proteins are synthesized with an N-terminal pre-sequence called a transit peptide. The transit peptide is necessary for and also sufficient for plastidial targeting and translocation initiation.

Nucleus-encoded chloroplast proteins are fully translated on free polysomes in the cytosol before their targeting to plastids. It is envisaged that some cytosolic factors exist,

recognizing and facilitating targeting of chloroplast precursor proteins to the plastid surface. Indeed, two cytosolic factors, 14-3-3 protein, in association with cytosolic Hsp70s, have been shown to associate with transit peptides in vitro and are suggested to be important for precursor targeting to plastids (May T et al., 2000; Waegemann K et al., 1996; Qbadou S et al., 2006).

After reaching the chloroplast surface, the transit peptide of a precursor is recognized by Toc159 in its GTP-bound state. GTP hydrolysis by Toc34 may modulate this recognition and/or the translocation of transit peptides to Toc75. This early recognition step most likely takes place on a Toc complex not yet assembled with Tic components. In the next step, a low concentration of ATP (less than 100 μM) results in translocation of the transit peptide across the outer envelope membrane through the Toc75 channel (Inoue H et al., 2008). The transit peptide is further translocated across the inner envelope membrane through the Tic20/Tic21 complex and bound by the N-terminal half of Tic110 stromal domain. When sufficient ATP is present in the stroma, translocon components located in the stroma get to work. Tic110, loaded with the transit peptide, recruits the Tic40 TPR domain to the C-terminal half of its stromal domain. Binding of Tic40 induces the release of the transit peptide from Tic110, and the transit peptide is cleaved by SPP. The Tic40 Hip/Hop domain then stimulates ATP hydrolysis by Hsp93, which pulls the processed mature protein into the stroma. Cpn60 may assist the folding of proteins after translocation. Tic40 dissociates from Hsp93 after ATP hydrolysis. Under normal growth conditions in the light, when the stromal ATP concentration is high, ADP on Hsp93 may quickly be exchanged with ATP and another cycle of translocation can begin (Chou M.L. et al., 2006). (Model-1)

Yu et al. have revealed that the precursor of AtAMY3 (99.7 kDa) has a predicted

N-terminal transit peptide for plastidial localization, and 93.5 kDa AtAMY3 is present in chloroplasts isolated from *Arabidopsis* leaves (Yu et al., 2005). In contrast to secretory α-amylase, plastidial AtAMY3 appears to be synthesized in the cytosol as a precursor with the transit peptide, imported through the Toc/Tic apparatus to the stroma, and then processed to the 93.5 kDa mature form.

Recently, however, trafficking of glycoproteins and proteins to the plastid via the endomembrane system has been reported (Jarvis, 2008). Several research groups have identified the presence of glycoproteins within the chloroplasts (Gaikwad et al., 1999; Asatsuma et al., 2005). Proteomic analysis of the *Arabidopsis* chloroplast has provided supporting information that there are many proteins (over 8% of the total) with predicted signal peptides for ER translocation (Kleffmann et al., 2004). A rice α-amylase (αAmy3) exhibited dual localization to plastids and extracellular compartments in plant cells (Chen et al., 1994; Chen et al., 2004). The αAmy3 protein had an ER signal sequence, but no predicted *N*-glycosylation site. The αAmy3 mRNA was translated in canine microsomes, and the translation products without the N-terminal extra-peptide were imported into the lumen of the organelle. Moreover, a reporter protein with the signal peptide of αAmy3 was mainly targeted to amyloplasts in rice cells (Chen et al., 2004). These results imply the existence of a signal peptide-dependent plastid protein transport pathway through the endomembrane system. More recently, convincing evidence has been presented for a traffic route from the ER-Golgi system to the plastid (Villarejo et al., 2005; Nanjo et al., 2006). The *Arabidopsis* carbonic anhydrase 1 (CAH1) that catalyzes the reversible reaction between carbon dioxide hydration and bicarbonate dehydration was found to localize in the chloroplast stroma despite having a signal sequence. The CAH1 protein has been

shown to contain five predicted *N*-glycosylation sites, and the mature chloroplast CAH1 was actually *N*-glycosylated. The oligosaccharide side chain of CAH1 bore β(1,2)-xylose and α (1,3)-fucose residues which are conjugated in the Golgi apparatus, in addition to the fact that the transport of CAH1 to chloroplast was reversibly prevented by a drug, Brefeldin A, that inhibits the ER-to-Golgi traffic (Villarejo et al., 2005). Rice nucleotide pyrophosphatase/phosphodiesterase 1 (NPP1), a recently identified enzyme which exhibits hydrolytic activity toward ADP-glucose linked to the starch biosynthesis, was a chloroplast glycoprotein conjugated with Concanavalin A-recognized *N*-linked oligosaccharide chains. Similarly, the enzyme glycoprotein was shown to be transported and localized to the chloroplasts from the secretory pathway via by the Brefeldin A-sensitive vesicular transport (Nanjo et al., 2006). These indicate that ER-to-Golgi traffic is essential for chloroplast targeting of glycoproteins in both monocot and dicot plants.

Our previous studies using transgenic rice plants with suppressed expression or overexpression of AmyI-1 revealed that the enzyme glycoprotein is involved in degradation of plastidial starch in living cells (Asatsuma et al., 2005; Asatsuma et al., 2006). Immunocytochemical analysis with specific anti-AmyI-1 antibodies, the expression and targeting of AmyI-1-GFP in re-differentiated green cells, and cell biochemical analysis of chloroplastic AmyI-1 demonstrated that AmyI-1 is present in the chloroplasts in rice leaves. The predicted precursor sequence of AmyI-1 contains the signal peptide for translocating the ER membrane, but no transit peptide. My thesis describes a unique transport system involved in the plastid-targeting of AmyI-1 glycoprotein and also identification of a plastid targeting signal of AmyI-1 common to both rice and onion cells.

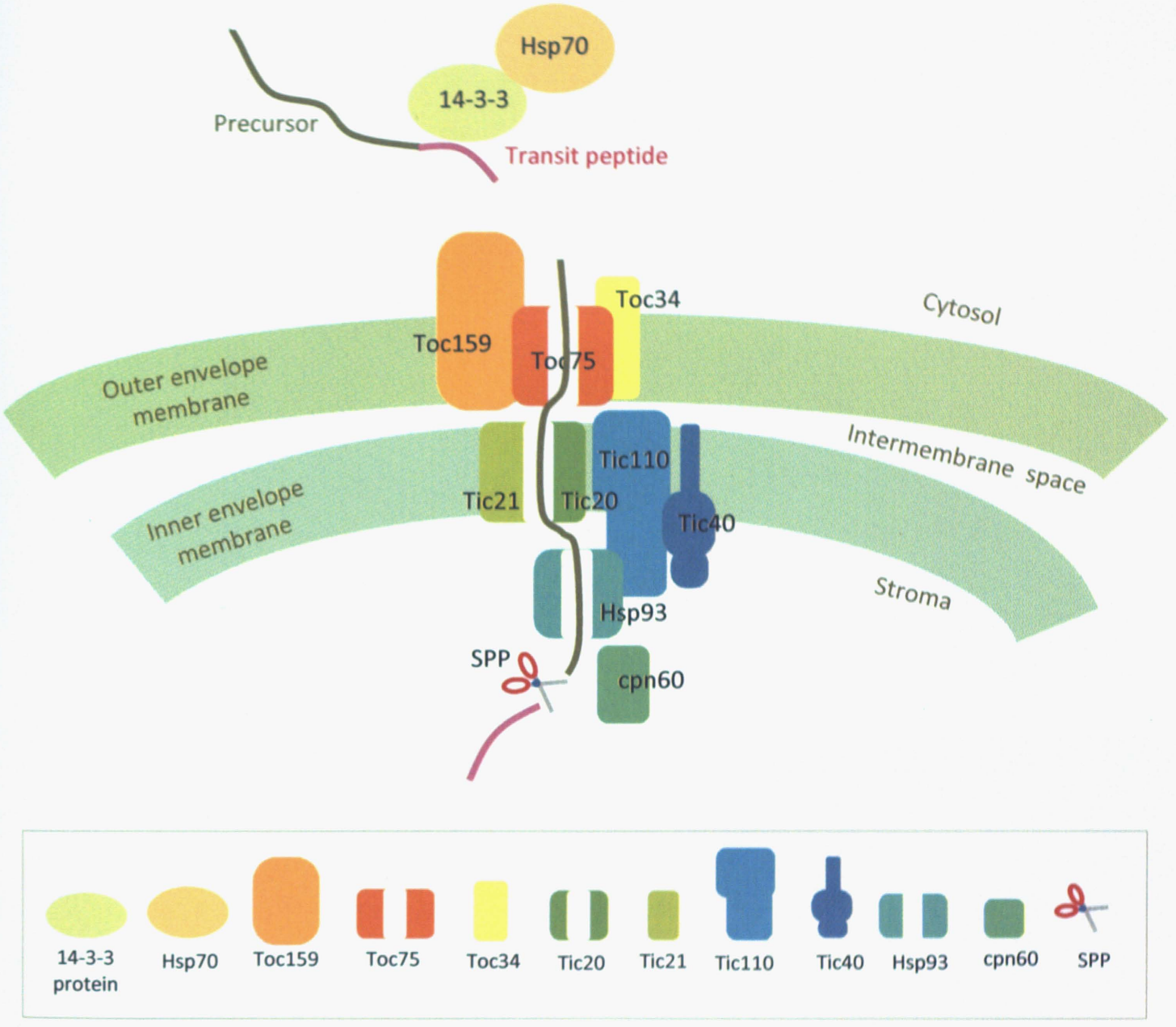

Model-1. A proposed model of protein translocation into the stroma.

Nucreus-encoded plastid proteins are fully translated on free polysomes in the cytosol and cytosolic factors like 14-3-3 proteins in association with cytosolic Hsp70s recognize and facilitate targeting of plastid precursor proteins to the plastid surface.

After reaching the plastid surface, the transit peptide is bound by Toc159 and Toc34. Then the transit peptide is translocated across the outer membrane through the Toc75 channel. The transit peptide is further translocated across the inner membrane and bound by Tic110. This step takes place at the Tic/Toc supercomplex. The transit peptide is cleaved by the SPP. Hsp93 pulls the processed mature protein into the stroma. Chaperonin cpn60 may assist the folding of proteins after translocation.

METHODS

Plant materials

Rice seeds (*Oryza sativa* L. cv. Nipponbare) were supplied by the Niigata Agricultural Research Institute (Niigata, Japan). The production of transgenic rice seed (A3-1 line) has been described previously (Asatsuma et al., 2005). Rice calli derived from the embryo portion of the seed were cultured as follows. About 2 g of rice callus cells were grown in a 500-ml Sakaguchi flask holding 120 ml of Murashige-Skoog (MS) medium containing 3% (w/v) sucrose, 2 mg/l 2,4-dichlorophenoxyacetic acid, and 5 mg/l thiamine-HCl, placed on a reciprocal shaker operated at 110 strokes/min with 70-mm amplitude, at 28 ˚C in darkness. Established suspension-cultured cells were subcultured at 7-day intervals. All the procedures were performed under aseptic conditions. Amylase activity and starch content were determined as described in earlier studies (Mitsui et al., 1996; Asatsuma et al., 2005).

Plasmid constructs

Primer sequences for PCR amplifications are given in Table 1. The constructions of pAmyI-1, pGFP and pAmyI-1-GFP have been described previously (Asatsuma et al., 2005). For DsRed2 expression in onion epidermal cells, the BamHI-SacI PCR-amplified fragment from pDsRed2 (Takara Bio, Ohtsu, Japan) was cloned into the same sites of pGFP to produce pDsRed. To create pWxTP-DsRed, we PCR-amplified the first 1–111 amino acid residues, including the transit peptide sequence, from the rice waxy gene (pWCW) (Klösgen and Weil, 1991; Itoh et al., 2003) with two flanking primers, and then digested the PCR product with BamHI. The BamHI-digested fragment was inserted into the same site as pDsRed. To construct pWxTP-GFP, we

further inserted the PCR-amplified *WxTP* fragment into the *BamHI* site of pGFP. We also used pST-mRFP (Kim et al., 2001; Latijnhouwers et al., 2005), pper-GFP (Mano et al., 2002) and pmt-GFP (Niwa et al., 1999) to visualize the trans-Golgi, peroxisomes and mitochondria, respectively. The dominant negative mutants of AtARF1 and constitutive active mutant of AtSAR1 (pMT121-AtARF1 T31N, pMT121-AtARF1 Q71L, pMT121-AtSAR1 H74L, respectively) were reported previously (Takeuchi et al., 2002). Double entry vector pdEV(WxTP-GFP)(AmyI-1) was created from pWxTP-GFP and pAmyI-I using the Gateway system according to the manufacturer's protocol (Invitrogen, Carlsbad, CA, USA).

Each full-length *AmyII-3, II-4, II-5,* and *II-6* was PCR-amplified using pAmyII-3, pAmyII-5, pAmyII-6 or pAmyII-4 (Asatsuma et al., 2006), as DNA template and flanking primer sets. To construct pAmy-GFP, the PCR-amplified AmyII-3 (identical to accession number M59352 except for there being no BamHI site), II-4, II-5 and II-6 were inserted into pGFP.

To construct a set of pAmyI-1(truncated)- and pAmyI-1(point-mutated)-GFPs, carboxyl-terminal truncated *AmyI-1* series (Δ34–428, Δ101–428, Δ201–428, Δ301–428, Δ304–428, Δ351–428, or Δ370–428) and point-mutated *AmyI-1* series (W302L, W302A, T307V, or G354N) were PCR-amplified using pAmyI-1 as the DNA template and specific primer sets, and then inserted into pGFP.

We PCR-amplified *AmyI-1(256-369)(Gly)$_4$* and *AmyI-1(287-369)(Gly)$_4$* from pAmyI-1 and *35S-AmyII-6(1-266)(no BamHI site)* from pAmyII-6-GFP with flanking primer sets. To construct pAmyII-6(1-266):AmyI-1(256-369)-GFP or pAmyII-6(1-266):AmyI-1(287-369)-GFP, the BamHI-KpnI-digested *AmyI-1(256-369)* or *AmyI-1(287-369)* and HindIII-BamHI-digested *35S-AmyII-6(1-266)* were

sequentially inserted into pGFP.

The construction of binary vectors pZH2B-35S-AmyI-1, pZH2B-35S-GFP and pZH2B-35S-AmyI-1-GFP has been described previously (Asatsuma et al., 2005). To create pZH2B-35S-AmyI-1(Δ101–428)-GFP and pZH2B-35S-AmyI-1(Δ370–428)-GFP, the *35S-AmyI-1(Δ101–428)-GFP* and *35S-AmyI-1(Δ370–428)-GFP* genes were PCR-amplified from pAmyI-1(Δ101–428)-GFP and pAmyI-1(Δ370-428)-GFP. The HindIII-NotI-digested fragment was then inserted into the same site of pZH2B. These vectors were transformed into competent cells of *Agrobacterium tumefaciens* stain EHA101 (Hood et al., 1986) and treated with 20 mM $CaCl_2$. *Agrobacterium*-mediated transformation and regeneration of rice plants were performed according to the methods described by Hiei et al. (1994).

Introduction of plasmids into onion cells

To introduce plasmid DNA into onion (*Allium cepa*) epidermal cells, the particle bombardment method was adopted using a helium-driven particle accelerator (PDS-1000/He; Bio-Rad, Hercules, CA) with all basic adjustments set according to the manufacturer's recommendations. Three μg of plasmid DNA in 10 μl distilled water was mixed with 10 μl of 60 mg/ml gold particles (diameter 1.0 μm) solution, 10 μl of 2.5 mM $CaCl_2$ and 4 μl of 0.1 M spermidine, and incubated for 30 min at room temperature. Gold particles coated with plasmid DNA were rinsed with cold ethanol and then gently suspended in 10 μl ethanol. The gold particles were bombarded twice into onion cells using the particle delivery system with 1100 psi rupture discs. The bombarded onion epidermal cells were cultured on 0.6% Gelrite with 2,4-D free MS medium at 25 °C in darkness.

Microscopy

Fluorescence microscopy: Images of GFP, DsRed and mRFP fluorescence in whole cells were observed using a microscopic setup composed of a microscope BX-61 (Olympus, Tokyo, Japan) and a cooled CCD camera (EM-CCD, Hamamatsu, Hamamatsu, Japan). An Hg lamp was used to excite the fluorescent proteins. The fluorescence of GFP was obtained by 470 to 490-nm excitation with 510 to 550-nm detection, and the fluorescence of DsRed and mRFP was effected by 520 to 550-nm excitation with $\geq$ 580-nm detection. Deconvolution was carried out using Lumina Vision imaging software (Mitani, Tokyo, Japan). Twenty to thirty images per cell, from the top to middle of the cell, every 1 to 2 μm, were taken and combined into one image.

Confocal laser scanning microscopy: Three microscopic settings were used for confocal fluorescence imaging of living cells. An Olympus FV300-BX-61 confocal laser scanning microscope (CLSM) was used for two-dimensional time-lapse observations, and an Olympus FV1000-IX-71 for three-dimensional time-lapse observations. In these CLSM settings, Ar and green He/Ne lasers were used to excite GFP at 488 nm and mRFP and DsRed at 543 nm. Reconstructions of 3D surface images were performed using an alpha-blend procedure using FV10-ASW imaging software (Olympus). A custom-made system produced by the Dynamic-Bio Project was used for higher-resolution and higher-speed observations (Figure 8B). In this system, an Olympus IX-70 microscope was equipped with a special high-signal-to-noise-ratio color confocal system (Yokogawa Electric), image intensifiers (Hamamatsu Photonics) and high-speed and ultra-high-sensitivity HARP cameras (NHK Engineering Services and Hitachi Kokusai Electric). At both settings, an Ar^+/Kr^+ laser (Melles Griot) was used to

excite GFP at 488 nm and mRFP at 568 nm simultaneously. For 3D imaging, the objective lens was oscillated vertically to the sample plane by means of a piezo actuator system (Yokogawa Electric). Collected pictures were analyzed using Volocity software (Improvision) (Matsuura-Tokita et al., 2006).

Quantitative analysis: The fluorescence intensity in plastids and in whole cells was determined using Lumina Vision imaging software. The background was always set at the maximum value of fluorescence intensity for the area in which no structural image was present. The area visualized with either WxTP-GFP or WxTP-DsRed was defined as the plastidial area. In analysis of the whole cell, each individual image from the top to the middle of the cell, 15–20 frames every 1–2 μm, was evaluated. To evaluate the plastid-targeting abilities of GFP-labeled proteins, we determined the ratio of the fluorescence intensity of GFP in the plastidial area provided with WxTP-DsRed to GFP in the whole cell ($GFP_{plastid}/GFP_{total}$). On the other hand, to estimate the incorporation of ST-mRFP into plastids, the ratio of the fluorescence intensity of RFP in the plastidial area provided with WxTP-GFP to RFP in the whole cell ($RFP_{plastid}/RFP_{total}$) was determined and compared. In the case of time-lapse experiments, the values of RFP fluorescence intensity by area unit of plastid visualized with WxTP-GFP (RFP intensity/μm^2 of plastid) were determined.

Electron microscopic studies

High-pressure frozen/freeze substituted cells: Rice wild-type and A3-1 cells constitutively and highly expressing AmyI-1 cultured in MS medium containing 3 % sucrose at 28 ˚C for 4 days were immediately placed on a flat specimen carrier and

frozen in a high-pressure freezer (EM-PACT; Leica Microsystems, Wetzlar, Germany). The frozen samples were fixed in anhydrous acetone containing 2% osmic acid (OsO_4) for 3–4 days at –80 °C for morphological observation, or fixed with anhydrous acetone containing 1% glutaraldehyde and 1% OsO_4 for 3–4 days at –80 °C for immunocytochemistry. The tubes containing the frozen samples were warmed at 3 °C/h to a temperature of –20 °C, at 1 °C/h from –20 °C to 4 °C, and kept for 2 h at 4 °C using an automatic freeze-substitution system (EM-AFS; Leica Microsystems). For morphological observation, the samples were stained with 1% tannic acid in acetone for 1 h at room temperature. The samples were then washed with 100% acetone and embedded in epoxy resin (TAAB, Aldermaston, UK). The fixed samples for immunocytochemistry were embedded in LR White resin (London Resin, Basingstoke, UK).

The ultra-thin sections for morphological and immunocytochemical observations were mounted on 400-mesh Cu and 600-mesh Ni grids, respectively. Immunocytochemical detection of AmyI-1 was performed according to Toyooka et al. (2009). The sections on Ni grids were treated with 10% BSA in Tris-buffered saline (TBS) for 30 min at room temperature. The sections were incubated with an affinity-purified polyclonal antibody toward AmyI-1 (1:100) in TBS. After washing with TBS, the sections were further incubated with 12-nm colloidal gold particles conjugated to goat anti-rabbit IgG (Jackson ImmunoResearch, West Grove, PA). The sections were washed with TBS and rinsed in distilled water. Both sections for morphological and immunochemical observations were finally stained with 4% aqueous uranyl acetate for 5 min and examined using a transmission electron microscope (JEM-1011: JEOL, Tokyo, Japan) at 80 kV. Images were acquired using a Gatan

DualView camera and Digital Micrograph software (Gatan, Warrendale, PA) or TEM films.

Unfrozen cells: Freshly harvested rice cells were fixed with 4 % (w/v) paraformaldehyde and 60 mM sucrose in 50 mM cacodylate buffer (pH 7.2) overnight at 4 °C. The samples were dehydrated and embedded in either epoxy or LR White resin, then cut into ultra-thin sections. In immunocytochemical detection of AmyI-1, the sections on Ni grids were washed with PBST containing 1 % BSA for 20 min and then incubated in a 1:100 dilution of anti-AmyI-1 antibodies or non-immune sera in PBST at 4 °C for 1h. The sections were washed with PBST for 20 min and then incubated with 10-nm colloidal gold-conjugated protein A at 4 °C for 30 min. The sections were washed with PBST and distilled water, then finally stained with uranyl acetate for 10 min and lead citrate for 2 min, sequentially. They were examined using a Hitachi H-600 transmission electron microscope at an accelerating voltage of 75 kV.

Accession Numbers

Rice α-amylase genes discussed in this study are as follows. Amy I-1 (AAA33885, M24286), II-3 (AAA33896, M59352), II-4 (AAA33886, M24287), II-5 (CAA39777, X56337), and II-6 (CAA39778, X56338).

Table 1: Primer sequences for PCR-amplification

Amplified DNA (Plasmid constructed)	DNA template	Primer sequences
WxTP	pWCW	5'-ctggatccatgtcggctctcaccacg-3'
(pWxTP-GFP, pWxTP-DsRed)		5'-tatggatccggcaggggggaggccaccgag-3'
AmyI-1	pAmyI-1	5'-atcgggatccatggtgaacaaacacttctt-3'
(pAmyI-1-GFP)		5'-aaggatccgcttttctcccagattgcgt-3'
AmyII-3	pAmyII-3	5'-aaggatccatgggcaagcaccatgtcac-3'
(pAmyII-3-GFP)		5'-ttggtaccatagtgctttctaccggca-3'
AmyII-4	pAmyII-4	5'-atcgggatccatgaagaacaccagcagc-3'
(pAmyII-4-GFP)		5'-aaggatcctaggtgccgccccgccgggac-3'
AmyII-5	pAmyII-5	5'-aaggatccatggcaaagcgcatagcctc-3'
(pAmyII-5-GFP)		5'-ttggatccatagtggtgccgccctgcagg-3'
AmyII-6	pAmyII-6	5'-taggatccatggcaaagcattccaccac-3'
(pAmyII-6-GFP)		5'-atggatccgtggcgccgccctgctggaac-3'
AmyI-1(⊿34-428)	pAmyI-1	5'-atcgggatccatggtgaacaaacacttctt-3'
(pAmyI-1(⊿34-428)-GFP)		5'-aaggatccgttgaatccctgaaacaggac-3'
AmyI-1(⊿101-428)	pAmyI-1	5'-atcgggatccatggtgaacaaacacttctt-3'
(pAmyI-1(⊿101-428)-GFP)		5'-aaggatccctcgatcagcgacttgagct-3'
AmyI-1(⊿201-428)	pAmyI-1	5'-atcgggatccatggtgaacaaacacttctt-3'
(pAmyI-1(⊿201-428)-GFP)		5'-aaggatccccacgcgtcgaagccgatgtc-3'
AmyI-1(⊿301-428)	pAmyI-1	5'-atcgggatccatggtgaacaaacacttctt-3'
(pAmyI-1(⊿301-428)-GFP)		5'-taggatcccccgatcatgccgggcgcctt-3'
AmyI-1(⊿304-428)	pAmyI-1	5'-atcgggatccatggtgaacaaacacttctt-3'
(pAmyI-1(⊿304-428)-GFP)		5'-aaggtacccggccaccacccgatcatgcc-3'
AmyI-1(⊿351-428)	pAmyI-1	5'-atcgggatccatggtgaacaaacacttctt-3'
(pAmyI-1(⊿351-428)-GFP)		5'-aaggtacccaaatggtcgtagaagatgca-3'
AmyI-1(⊿370-428)	pAmyI-1	5'-atcgggatccatggtgaacaaacacttctt-3'
(pAmyI-1(⊿370-428)-GFP)		5'-aaggatccctgccggtttctgattgaca-3'
AmyI-1(W302A)	pAmyI-1	5'-gcgcccggcatgatcgggtgggcgccggccaaggcgacgacc-3'
(pAmyI-1(W302A)-GFP)		5'-ggtcgtcgccttggccggcgcccacccgatcatgccgggcgc-3'
AmyI-1(W302L)	pAmyI-1	5'-atgatcgggtggctgccggccaaggcg-3'
(pAmyI-1(W302L)-GFP)		5'-cgccttggccggcagccacccgatcat-3'
AmyI-1(T307V)	pAmyI-1	5'-ccggccaaggcggtgaccttcgtcgac-3'
(pAmyI-1(T307V)-GFP)		5'-gtcgacgaaggtcaccgccttggccgg-3'
AmyI-1(G354N)	pAmyI-1	5'-ttcttcgattggaatctcaaggtggtg-3'
(pAmyI-1(G354N)-GFP)		5'-ctcctccttgagattccaatcgaagaa-3'
AmyI-1(256-369)$(Gly)_4$	pAmyI-1	5'-aaggatccgtcgatcgtgtcggcggcgcc-3'
(pAmyI-1(256-369)-GFP)		5'-ataggtacccccgccgccccccctgccggtttctgattga-3'
AmyI-1(256-369)$(Gly)_4$	pAmyI-1	5'-aaggatccctccgcggcgaggacggcaag-3'
(pAmyI-1(287-369)-GFP)		5'-ataggtacccccgccgccccccctgccggtttctgattga-3'
35S-(BamHI to ApaI)-AmyII-6	pAmyII-6-GFP	5'-ggggactctagagggcccatggcaaagcat-3'
(p35S-(BamHI to ApaI)-AmyII-6-GFP)		5'-atgctttgccatgggccctctagagtcccc-3'
35S-(BamHI to ApaI)-AmyII-6(1-266)	p35S-(BamHI to ApaI)-AmyII-6-GFP	5'-gcgcaagcttagattagccttttcaatttc-3'
(pAmyII-6(1-266)/AmyI-1(256-369)GFP		5'-taaggatcccgatgcagggccaccga-3'
35S-(BamHI to ApaI)-AmyII-6(1-266)	p35S-(BamHI to ApaI)-AmyII-6-GFP	5'-gcgcaagcttagattagccttttcaatttc-3'
(pAmyII-6(1-266)/AmyI-1(287-369)GFP		5'-taaggatcccgatgcagggccaccga-3'

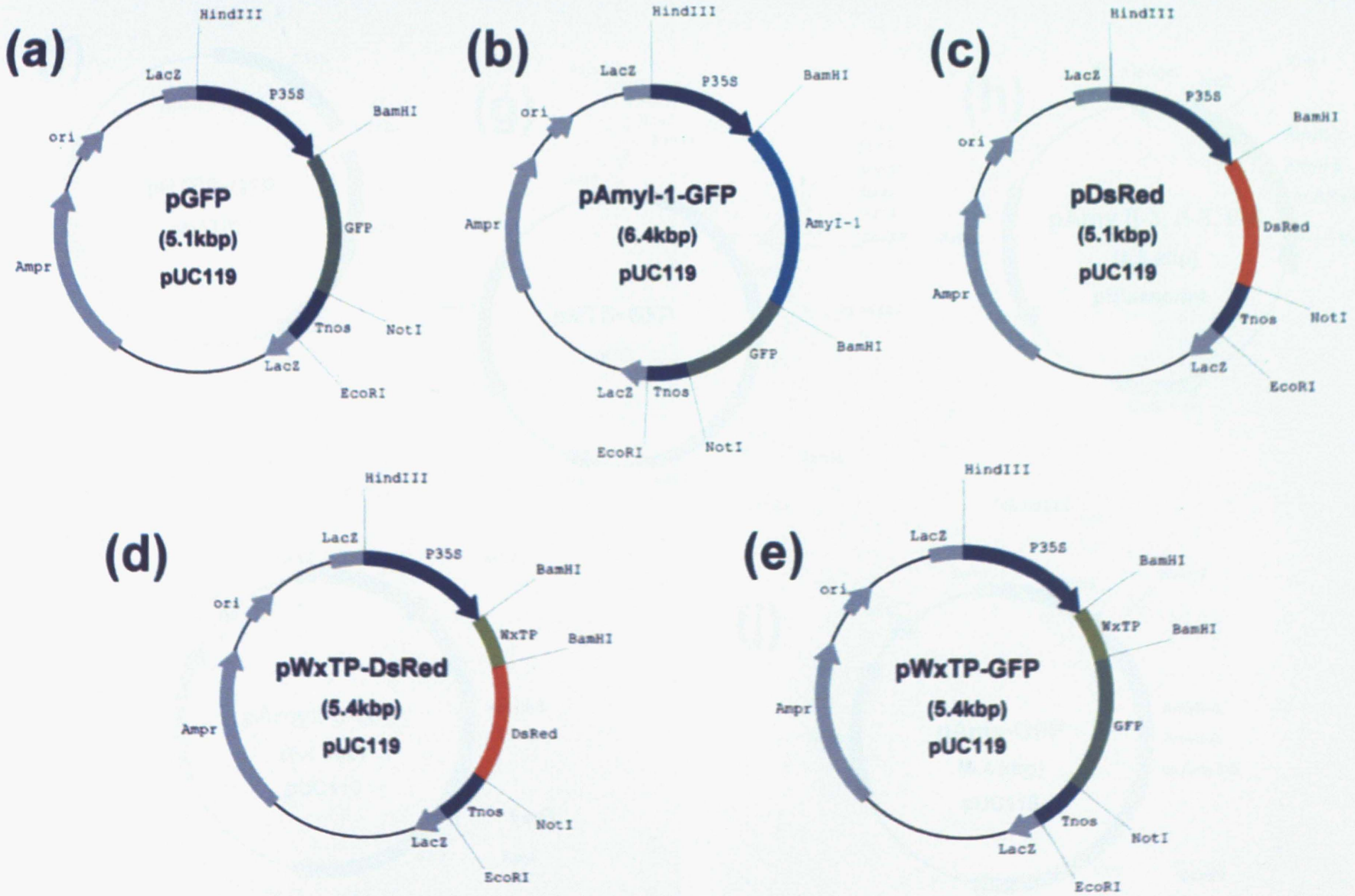

Plasmid map-1

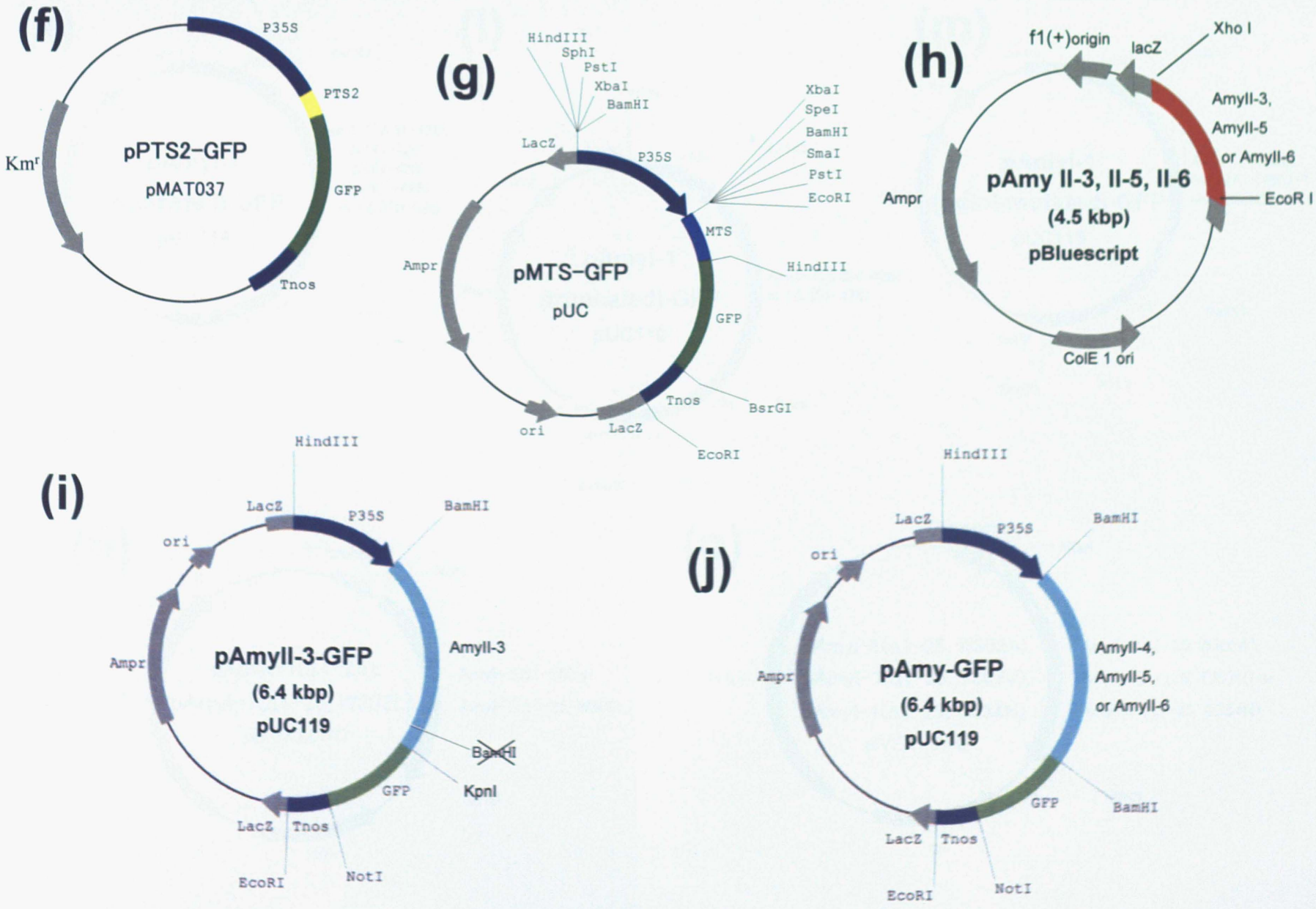

Plasmid map-2

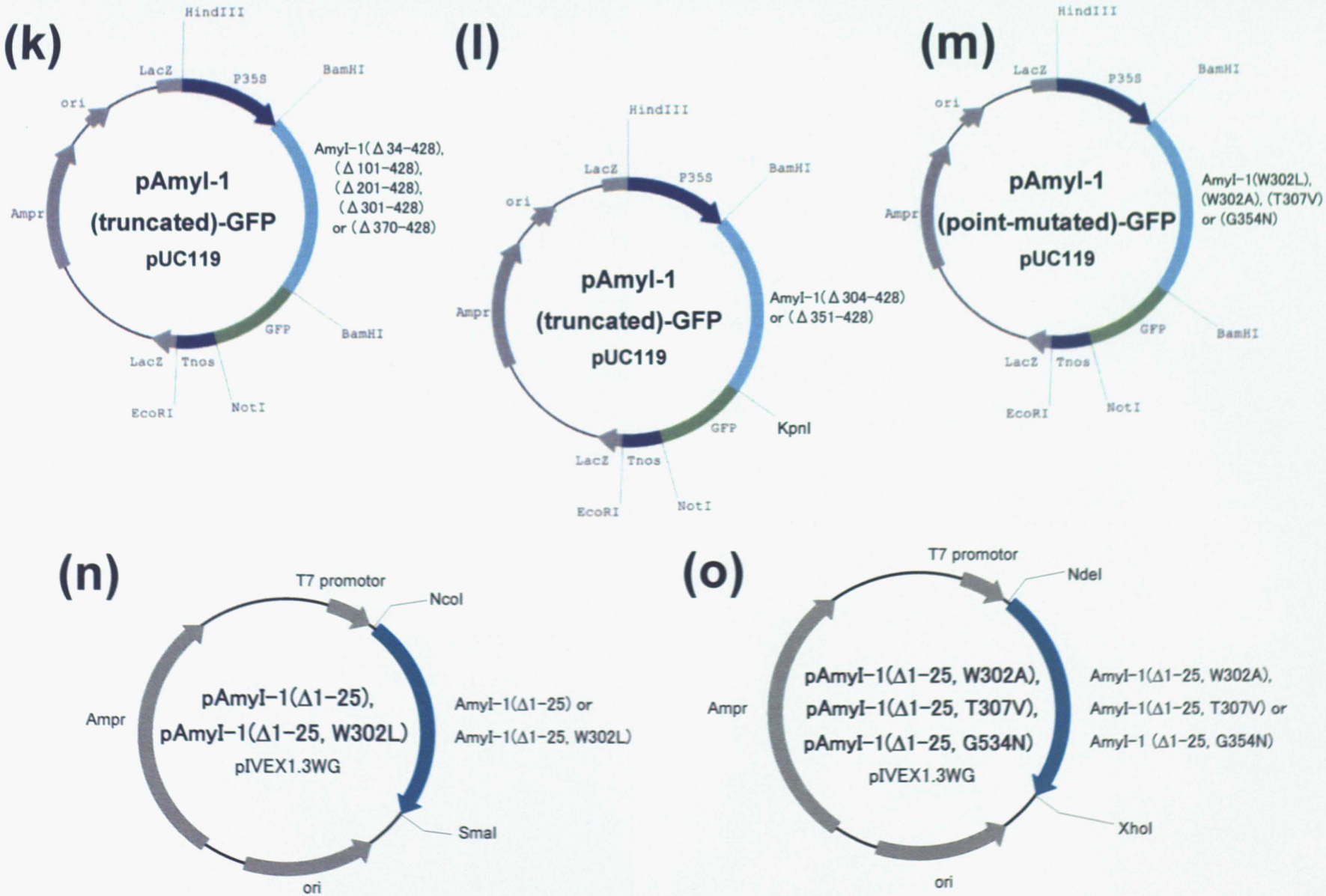

Plasmid map-3

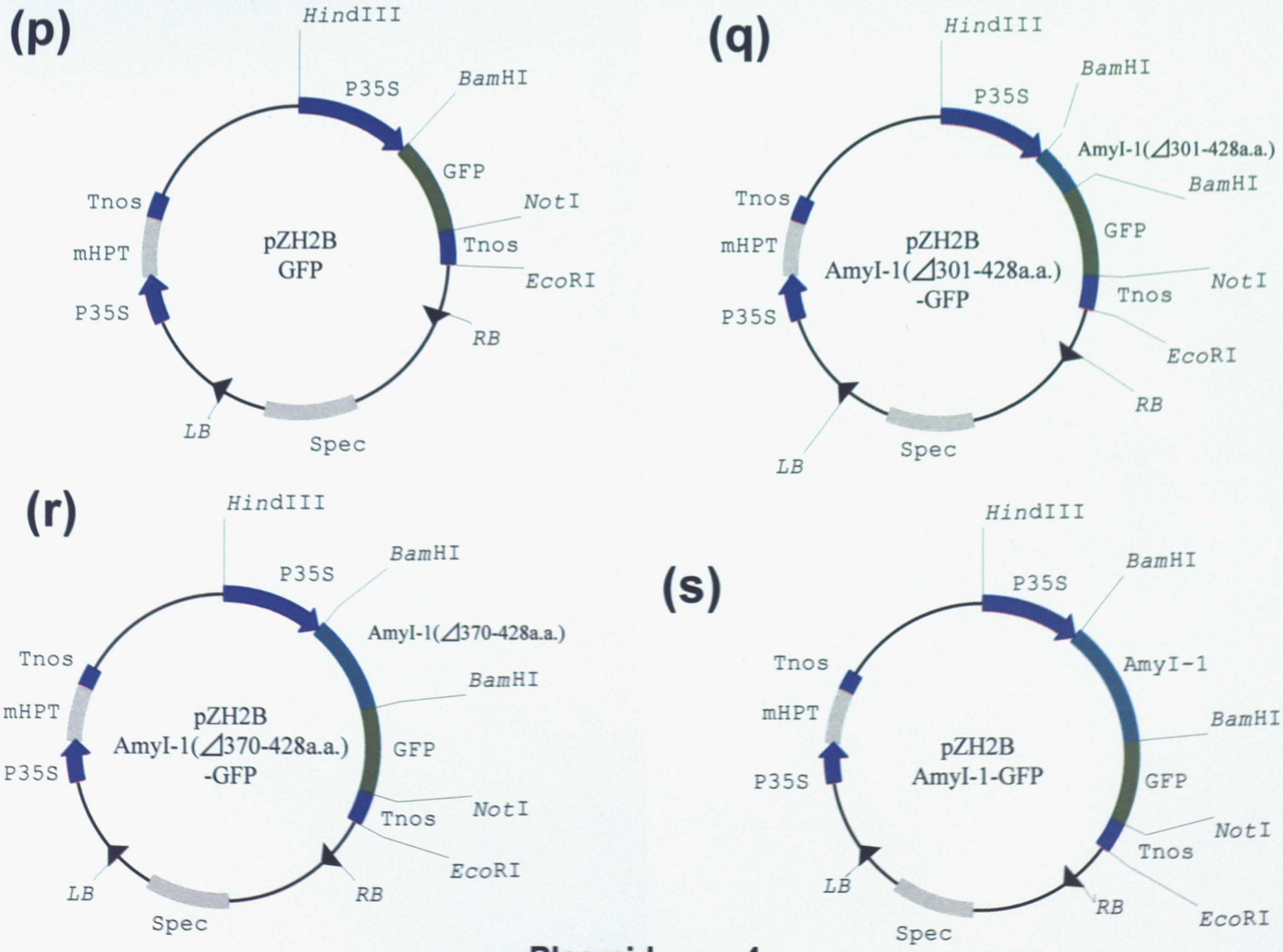

Plasmid map-4

RESULT

AmyI-1 degrades starch granules in living rice cells

α-Amylases in rice are polymorphic enzymes. The α-amylase isoforms AmyI-1 (*RAmy1A, aaAmy7*), II-3 (*RAmy3E, aaAmy8*), II-4 (*RAmy3D, aaAmy3*) and II-5/6 (*RAmy3B/3C, aaAmy6*) are extensively expressed in rice plant and tissue culture (Mitsui et al., 1996; Nanjo et al., 2004). The amino acid sequence alignment of these isoforms with a possible secondary structure of AmyI-1 predicted by the Phyre program (Bennett-Lovsey et al., 2008) is shown in Figure 1. A typical N-terminal signal peptide for ER membrane translocation was confirmed in all precursor forms of these isoforms. The oligosaccharide structure and its conjugating site for AmyI-1 have been determined (Hayashi et al., 1990, Terashima et al., 1994). Thus, there is no doubt that AmyI-1 is a secretory glycoprotein.

Rice callus cells derived from the embryo portion of the seed actively synthesize and secrete α-amylases under sugar-starved conditions, whereas sucrose supplementation almost entirely prevents the extracellular liberation of AmyI-1: a significant amount of the enzyme molecule is retained intracellularly (Mitsui et al., 1999). We employed callus cells derived from transgenic rice seed (A3-1 line) with constitutively high expression of AmyI-1 to examine the localization and function of AmyI-1 by electron microscopy. In contrast to the presence of rice starch granules in the amyloplasts of wild-type cells (Figure 2A), the amyloplasts of A3-1 had slim starch granules with large interspaces under sucrose-supplemented conditions (Figure 2B). Quantitative measurements showed that the

starch content in the callus cells overexpressing AmyI-1 was reduced to approximately half of that in the wild type (Figure 2F). To determine the subcellular localization of AmyI-1, we performed immunocytochemical analyses on ultrathin sections of both wild-type and A3-1 cells using anti-AmyI-1 antibodies. Some immuno-gold particles that exhibit the occurrence of AmyI-1, visualized as black dots, were detected in the amyloplasts of wild-type cells (Figure 2C). Much more heavy and clustered labeling was deposited in the amyloplasts and small membrane vesicles of A3-1 cells (Figure 2D). The positive signal was also detected in the vacuole. It has been recently reported that ribulose-1,5-bisphosphate carboxylase/oxygenase (Rubisco) and stromal-targeted fluorescent proteins can be mobilized to the vacuole through an autophagic process (Ishida et al., 2008). The AmyI-1 proteins in the vacuole may come from the plastids. Sections treated with the preimmune sera showed no signal (Figure 2E). It is evident from these results that AmyI-1 targets and degrades the starch granules in the amyloplasts of living callus cells.

AmyI-1 contains a plastid-targeting signal common to both rice and onion cells

To characterize the nature of plastid localization of AmyI-1 in details, we carried out transient expression of α-amylase isoforms (I-1, II-3, II-4, II-5 and II-6) fused with green fluorescent protein (GFP) using onion epidermal cells. Since onion cells have no chlorophyllous autofluorescence, it is necessary to visualize the plastids for evaluating the plastid targeting of Amy-GFP. The transit peptide of Waxy (Klösgen and Weil, 1991) fused to either GFP or red fluorescence protein from *Discosoma sp.* (DsRed) was expressed in onion epidermal cells using the particle bombardment procedure. The plastids with stromules were clearly visualized with two fluorescence proteins, WxTP-GFP and WxTP-DsRed (Figure 3), and their distributions were clearly distinguishable from the other organelles, peroxisomes and mitochondria, visualized with per-GFP and mt-GFP, respectively (Figure 4). Thus, WxTP-GFP and WxTP-DsRed were shown to be suitable plastid markers in onion cells.

AmyI-1-GFP was simultaneously expressed with a plastid marker, WxTP-DsRed. As shown in Figure 5A, a large portion of AmyI-1-GFP fluorescence overlapped with the plastids visualized by WxTP-DsRed. Some types of GFP fluorescence, however, indicated the ER-Golgi network in addition to the inside of the plastids in the cells (Figure 5D upper), suggesting that AmyI-1 is transported to plastids from ER-Golgi in onion cells. Distribution of the other rice amylase isoform was also tested, but unlike in the AmyI-1-GFP, the

fluorescence of AmyII-3-, AmyII-4-, AmyII-5- and AmyII-6-GFP rarely merged with the plastid marker (Figure 5B right and Figure 6A), and was constantly detected in the ER-Golgi network (Figure 5D lower). Statistical analysis confirmed that the targeting abilities of the other isoforms are much lower than AmyI-1 (Figure 5E, Figure 6), indicating that the plastid targeting of AmyI-1 is not a result of artificial overexpression of secretory proteins. AmyI-1 clearly possesses a plastid-targeting signal common to both rice and onion cells.

Membrane trafficking is necessary for plastid targeting of AmyI-1

ARF1 and SAR1 GTPases are essential for membrane trafficking between the ER and the Golgi apparatus in tobacco and *Arabidopsis* cells (Takeuchi et al., 2000; Takeuchi et al., 2002). Expression of dominant negative or constitutive active mutants of ARF1 and SAR1, which are defective in GTPase cycling, inhibits the ER-to-Golgi traffic. Golgi-resident proteins and secretory and vacuolar proteins are therefore retained in the ER network structure in the presence of such mutants. The effects of AtARF1(T31N), AtARF1(Q71L), and AtSAR1(H74L) mutants on the plastid targeting of AmyI-1-GFP were tested. The transport of AmyI-1-GFP into plastids was severely inhibited by the ARF1 and SAR1 mutants and the fluorescent proteins remained in the ER network structure (Figure 5C). Punctate structures in addition to the ER network were also fluorescent, probably representing ER exit sites; they never overlapped with plastids.

A statistical analysis showed that the transport activity of AmyI-1-GFP into plastids was significantly reduced in the ARF1 and SAR1 mutants (Figure 5E). As controls, the effects of these mutants on the localization of a trans-Golgi marker (transmembrane domain of sialyltransferase fused to the monomeric red fluorescent protein ST-mRFP) (Kim et al., 2001; Latijnhouwers et al., 2005) were tested. The trans-Golgi marker in the cells expressing AtARF1(T31N), AtARF1(Q71L) or AtSAR1(H74L) was relocated to the ER network (Figure 7A). By contrast, as would be expected, these mutants exhibited no

significant effect on the behavior of plastidial (WxTP-GFP), peroxisomal (per-GFP, the peroxisomal targeting signal 2 fused with GFP) or mitochondrial (mt-GFP, the presequence of the gg subunit of Arabidopsis F1-ATPase fused with GFP) markers (Figure 7B to D).

We previously demonstrated that another rice N-glycosylated glycoprotein, nucleotide pyrophosphatase/phosphodiesterase (NPP1), is transported from the secretory pathway to the chloroplast (Nanjo et al., 2006). α-Carbonic anhydrase was also reported to be *N*-glycosylated and transported to chloroplasts in *Arabidopsis* leaves and suspension-cultured cells (Villarejo et al., 2005). Both glycoproteins were targeted to plastids in a Brefeldin A (BFA)-sensitive manner (Ritzenthaler et al., 2002). Overall, these results strongly suggest that the membrane trafficking from the ER is necessary for the plastid targeting of these glycoproteins.

Golgi-to-plastid traffic

The mammalian Golgi apparatus has been shown to cluster and form a juxta- or perinuclear network in the cells. In contrast, plant Golgi stacks are dispersed singly or in small clusters throughout the cytoplasm and show active and "stop-and-go" tumbling movements along actin microfilaments (Nebenführ et al., 1999). The active movement of plant Golgi stacks suggests that the Golgi stack itself serves as a cargo container. If a genuine route from the Golgi complex to plastids exists, we consider it possible that these two organelles might be in constant communication. To test this idea, we performed high-speed two-dimensional and three-dimensional time-lapse analyses using confocal laser scanning microscopy. When ST-mRFP and WxTP-GFP were simultaneously expressed together with AmyI-1, which would activate Golgi-to-plastid traffic in onion cells, significant merging of ST-mRFP with the GFP-labeled plastids was observed (Figures 8 and 9). Moreover, the time-lapse scans caught several dramatic scenes: (a) The Golgi bodies made a soft landing on the surface of the plastid (Figure 8A). (b) Close contact between the two organelles was occasionally observed (Figure 8B). (c) Small membrane vesicles derived from the trans-Golgi were detected on the surface of the plastid (Figure 9C and D). Intriguingly, the fluorescent membrane vesicles did not stay long on the envelope membranes. They were eventually relocated to the interior of the plastid (Figure 9E).

In the cells expressing ST-mRFP and WxTP-GFP without AmyI-1, such overlapping

of mRFP and GFP appeared to be less frequent (Figure 9A and F). Three-dimensional time-lapse imaging showed that even without AmyI-1 expression, the ST-mRFP-labeled Golgi adheres to the surface of plastids and stromules (Figure 9B). The incorporation of ST-mRFP into plastids still occurred (Figure 10), albeit at lower frequency. In addition to these, Golgi-to-plastid trafficking was noticeably prevented by the expression of either AtARF1(T31N) or AtSAR1(Q74L) (Figure 9F). Taken together, we strongly inferred that Golgi-to-plastid basal communication occurs under tranquil physiological conditions, and that the AmyI-1 co-expression enhances the flow of Golgi-to-plastid traffic and activates the communication between two organelles in the cell.

To clarify the precise mechanism of Golgi-to-plastid traffic, electron microscopic studies were carried out of suspension-cultured cells derived from transgenic rice seed (A3-1 line) with a constitutively high expression of AmyI-1 using high-pressure frozen/freeze-substituted techniques (Toyooka et al., 2006). In the electron microscopic images, it was frequently observed that small membrane vesicles, perhaps derived from the Golgi apparatus stayed by their side, adhered to the envelope membrane of plastids (Figure 11A). Tight association of the Golgi stacks with the envelope membrane was also observed in the same cells (Figure 11C). As shown in Figures 11A to C, membrane vesicles are apparently taken up into the plastid, possibly passing through the envelope membranes. Furthermore, immunological staining of ultrathin sections with anti-AmyI-1 antibodies revealed the presence of AmyI-1 in both the Golgi apparatus and the plastids (Figure 11D

and E), and, moreover, the clustering of AmyI-1 proteins on and beneath the envelope membrane, representing the instant of plastid entry of clustered AmyI-1 proteins (Figure 11E).

Characterization of the plastid-targeting signal of AmyI-1

The majority of chloroplast proteins are synthesized in the cytosol as precursors with an N-terminal transit peptide and imported post-translationally through the Toc/Tic complex into the organelle. As described above, however, the predicted precursor sequence of AmyI-1 contains no transit peptides for plastidial localization (Figure 1). To identify the plastid-targeting signal of AmyI-1, the transient expression and localization of a series of carboxyl-terminal truncated AmyI-1-GFP fusion proteins was examined in bombarded onion cells. The predicted signal peptidase cleavage site is the amino-terminal side of Gln^{26}. AmyI-1(Δ34–428) includes only the N-terminal ER signal peptide of AmyI-1. The obtained results clearly indicate that AmyI-1 cannot be targeted to the plastid by the signal peptide alone (Figure 12A and B). We thus conclude that the signal peptide of AmyI-1 is necessary to enter the secretory pathway but is not sufficient for plastid-targeting.

Like the barley α-amylase structure (Robert *et al.*, 2005), AmyI-1 appears to be composed of a large central domain of $(baba)_8$-barrels (A domain), a loop domain (B domain) and a C-terminal domain forming a five-stranded, anti-parallel bb-sheet (C domain). AmyI-1(Δ370–428) contains the full $(\beta\alpha\beta\alpha)_8$-barrel domain A and the loop domain B, but lacks the C domain. As shown in Figure 12A and B, AmyI-1(Δ370–428)-GFP fusion protein was normally targeted into the plastids like the full length AmyI-1. Further carboxyl-terminal deletion of AmyI-1 gave rise to the gradual loss

of plastid targeting ability, and AmyI-1(Δ301–428) exhibited no plastid targeting. This indicates the importance of the peptide region from Trp^{301} to Gln^{369} for plastid targeting of AmyI-1. A putative surface starch-binding, site Typ^{301}-Trp^{302}, and substrate binding subsites and catalytic residue in the active site cleft (His^{313}, Asp^{314}, Gln^{319}) were located in this region (Søgaard et al., 1993).

Amino acid sequence alignment of Amy isoforms revealed that AmyI-1 polypeptide has 12 unique amino acid residues in the region from 301 to 369 (Figure 1). Of these amino acid residues, we selected Trp^{302}, Thr^{307} and Gly^{354} located in different areas in the three-dimensional structure of the protein for the next site-directed mutagenesis experiments. The substitution of Ala or Leu for Trp^{302} strongly arrested the targeting of AmyI-1-GFP into the plastids. The substitution of Val for Thr^{307} or Asn for Gly^{354} also arrested the plastid targeting of AmyI-1-GFP, as in the W302A and W302L mutations (Figure 12A and C). Furthermore, the chimera proteins of AmyII-6(1-266): AmyI-1(256-369) and AmyII-6(1-266):AmyI-1(287-369) failed to localize in the plastids (Figure 13). Judging from these results, we infer that conformational changes in the region from Trp^{301} to Gln^{369} influence the targeting ability.

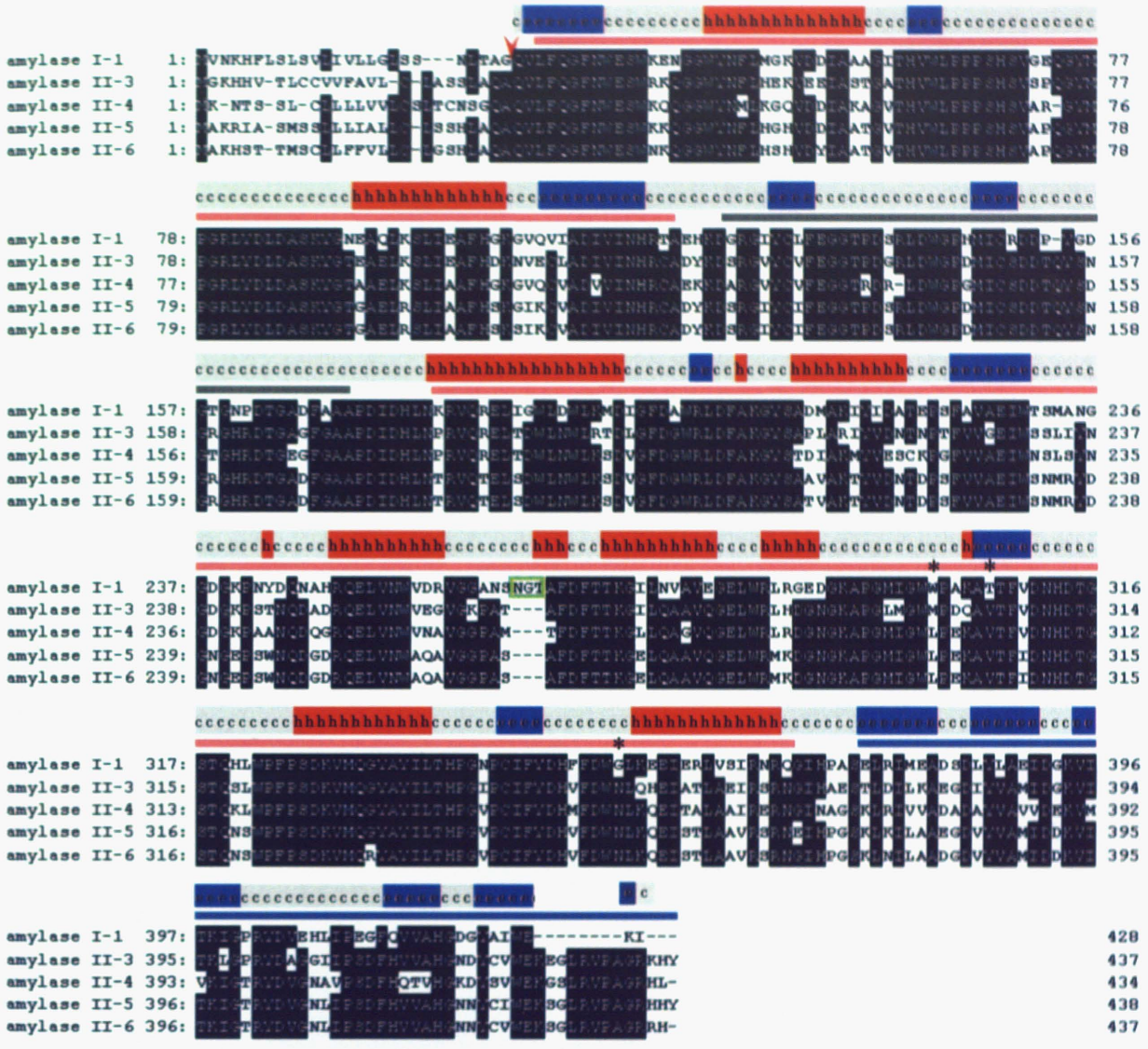

Figure 1. Amino acid sequence alignments of rice α-amylase isoforms.

Arrowhead indicates predicted cleavage sites, open green box shows a consensus sequence of *N*-glycosylation site, and conserved amino acids are black-boxed. A possible secondary structure of Amyl-1 predicted by the Phyre program is represented on the top of sequence alignment: h, α helix; e, β strand; c, coil. Red, gray and blue underlines are A, B and C domains, respectively.

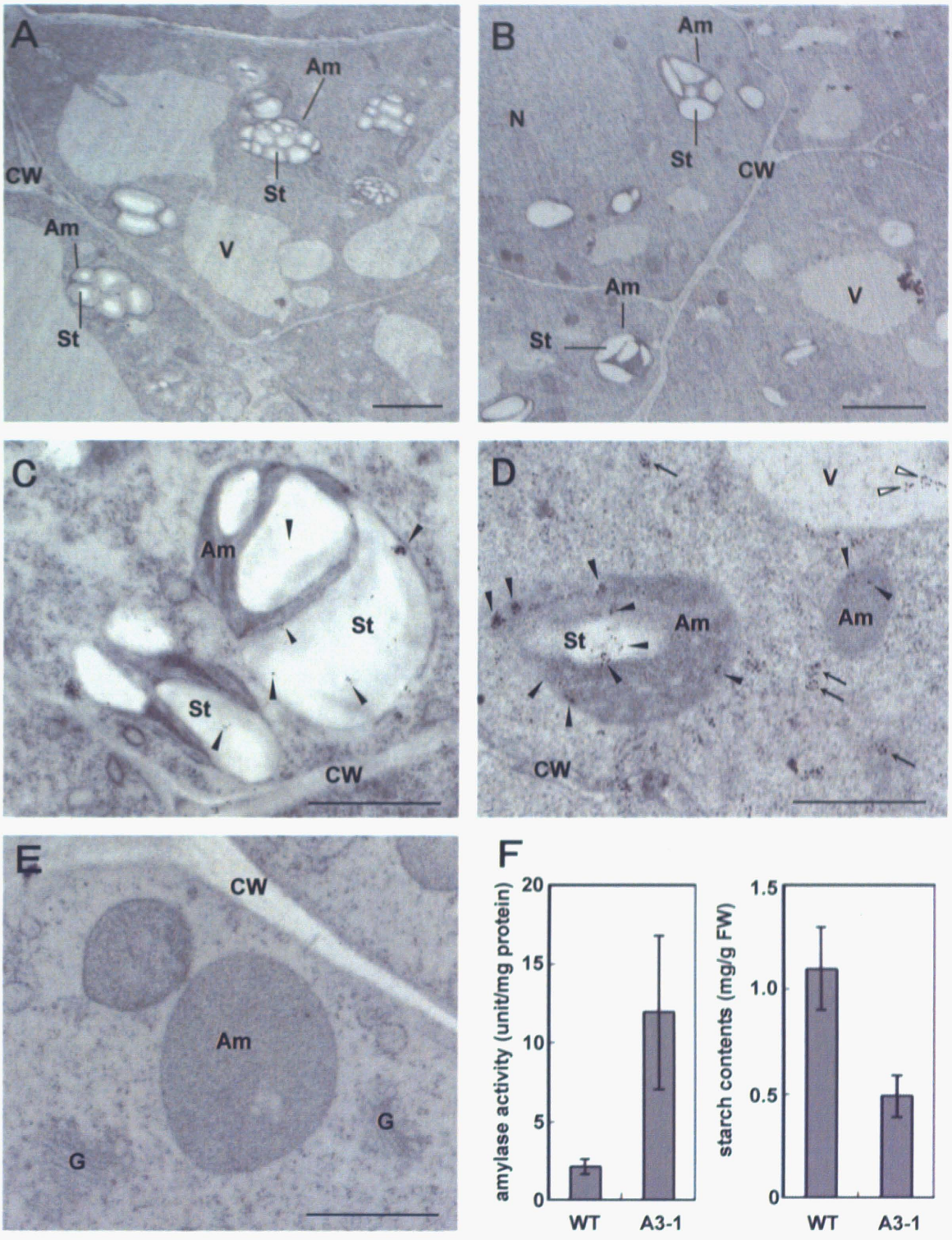
A
Am
CW
St
Am
V
St
B
Am
N
St
CW
Am
V
St
C
Am
St
St
CW
D
V
St
Am
Am
CW
E
CW
Am
G
G
F
amylase activity (unit/mg protein)
20
15
10
5
0
WT
A3-1
starch contents (mg/g FW)
1.5
1.0
0.5
0
WT
A3-1

Figure 2

Figure 2. Electron microscopy and biochemical characterization of rice A3-1 callus cells constitutively and highly expressing Amyl-1 under sugar-supplemented conditions.

Wild-type **([A]** and **[C])** and A3-1 **([B]** and **[D]** and **[E])** cells cultured in MS medium containing 3 % sucrose at 28 ˚C for 4 days were immediately subjected to fixation.
(A) and **(B)** Morphological observations.
(C) to **(E)** Immunocytochemical observations. The ultra-thin sections were incubated with either an affinity-purified polyclonal antibody toward Amyl-1 **([C]** and **[D])** or preimmune serum **[E]** and 10-nm colloidal gold-conjugated protein A, sequentially. Arrows, closed and open arrowheads indicate immunogold signals of Amyl-1 in small vesicle, amyloplast and vacuole, respectively. G, Golgi; Am, amyloplast; St, starch; CW, cell wall; V, vacuole; N, nucleus. Bars represent 1 μm.
(F) Quantitative data of amylase activity and starch content in wild-type and A3-1 cells. Values show mean ± s.d. obtained from three independent experiments.

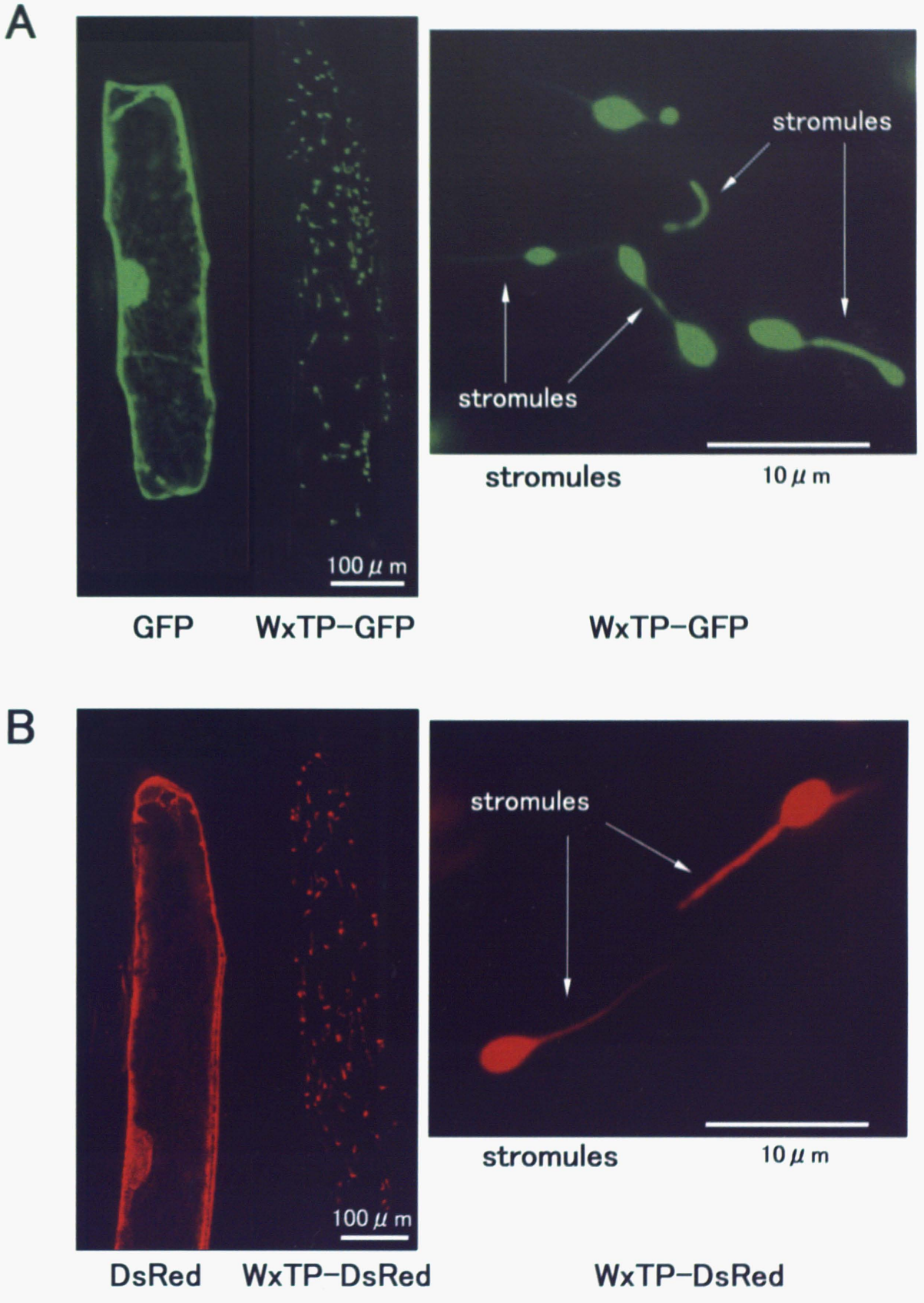
A
100 μ m
stromules
stromules
stromules
10 μ m
GFP
WxTP-GFP
WxTP-GFP
B
100 μ m
stromules
stromules
10 μ m
DsRed
WxTP-DsRed
WxTP-DsRed

Figure 3

Figure 3. Fluorescence images in onion epidermal cells expressing either GFP, DsRed, WxTP-GFP or WxTP-DsRed.

(A) *GFP* and *WxTP-GFP* bombarded cells. **(B)** *DsRed* and *WxTP-DsRed* bombarded cells. The epidermal cells were incubated on 0.6% gelrite with 2,4-D-free Murashige-Skoog (MS) medium for 24 h at 25 °C in darkness. Images of GFP and DsRed were observed using a microscopic setting composed of a BX-61 microscope (Olympus, Tokyo, Japan) and a cooled CoolSnap-*fx* CCD camera (Photometrics). In this setting, an Hg lamp was used to excite the fluorescent proteins. The fluorescence of GFP was obtained by 470 to 490-nm excitation and 510 to 550-nm detection, and that of DsRed was by 520 to 550-nm excitation and ≥ 580-nm detection. Deconvolution was carried out using Lumina Vision imaging software (Mitani, Tokyo, Japan). In a whole cell, 15 to 20 images per cell, from the top to middle of the cell, every 1 to 2 μm, were taken and combined into one image. The right-hand panels represent the fluorescent plastids in close-up. Plastids with stromules were similarly visualized by WxTP-GFP and WxTP-DsRed.

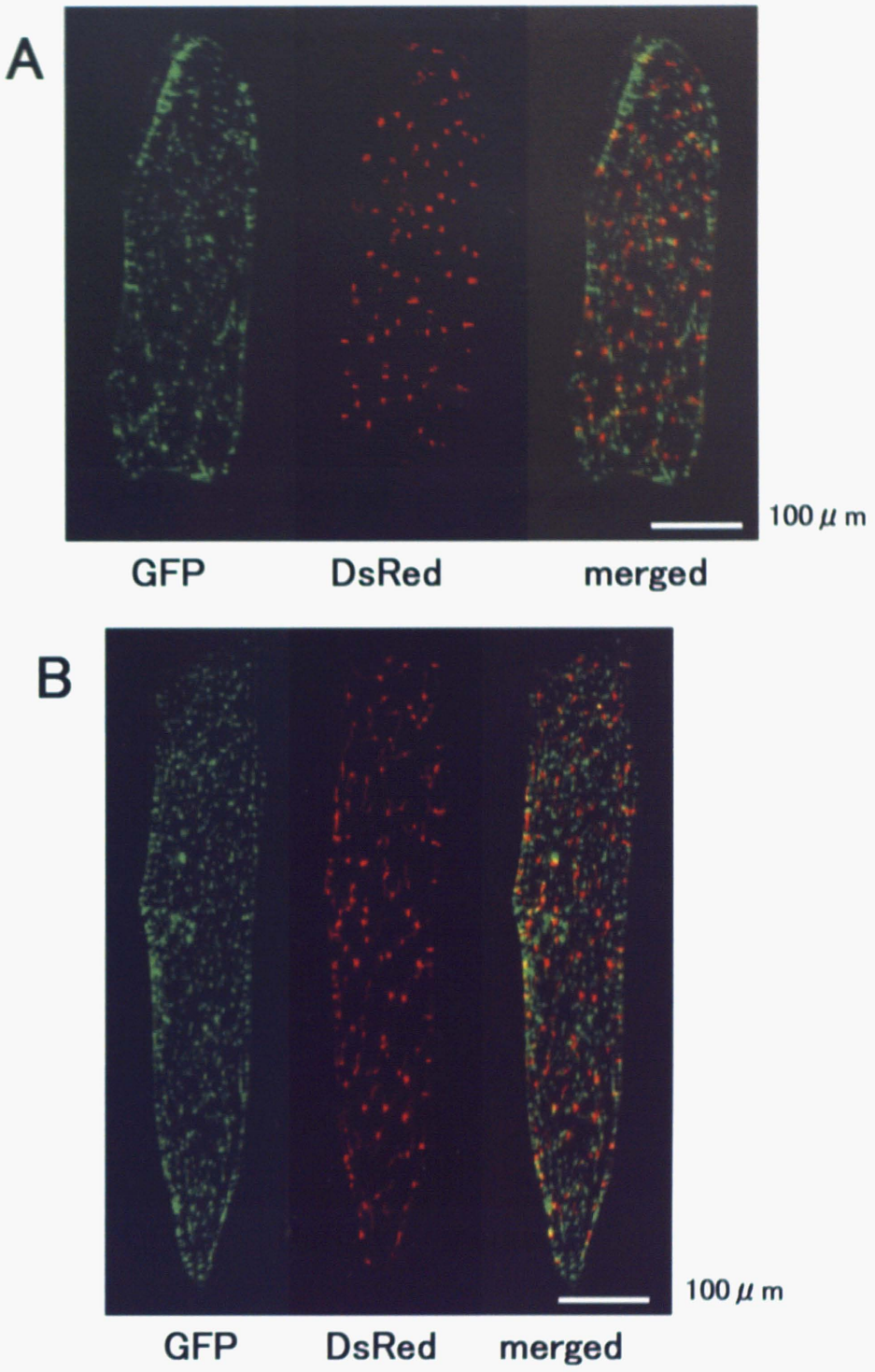

Figure 4. Fluorescence images in onion cells simultaneously expressing WxTP-DsRed with per-GFP or mt-GFP

(A) *WxTP-DsRed* and *per-GFP* (the peroxisomal targeting signal 2 fused with GFP) bombarded cell. **(B)***WxTP-DsRed* and *mt-GFP* (the presequence of the g subunit of Arabidopsis F1-ATPase fused with GFP) bombarded cell. Images were obtained as described in the legend for Supplemental Figure 1. The results show that the distribution of WxTP-DsRed is clearly distinguishable from those of per-GFP and mt-GFP, the peroxisome and mitochondria markers not merging to the plastid marker.

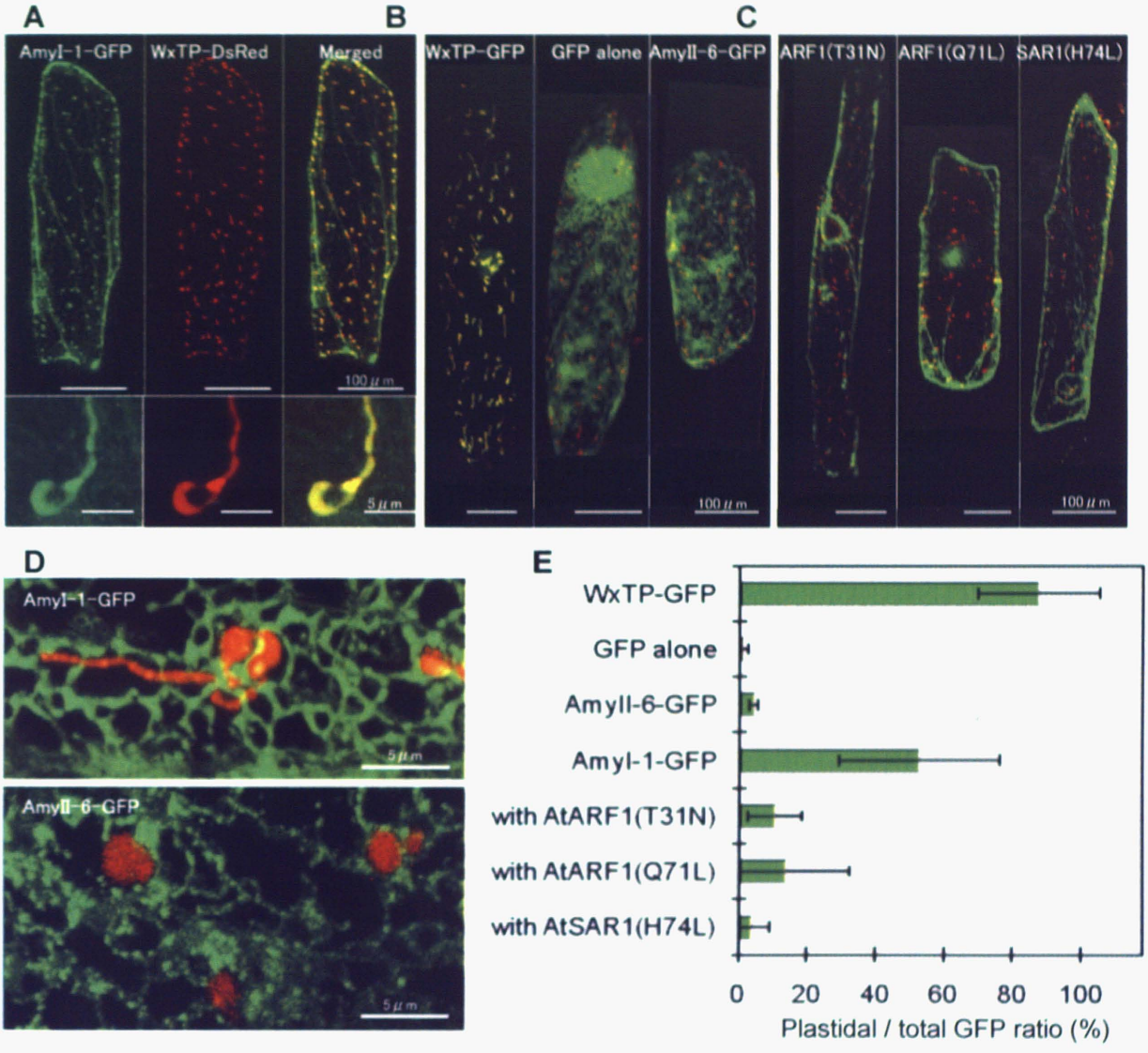
A
B
C
AmyI-1-GFP
WxTP-DsRed
Merged
100 μm
5 μm
WxTP-GFP
GFP alone
AmyII-6-GFP
100 μm
ARF1(T31N)
ARF1(Q71L)
SAR1(H74L)
100 μm
D
AmyI-1-GFP
5 μm
AmyII-6-GFP
5 μm
E
WxTP-GFP
GFP alone
AmyII-6-GFP
AmyI-1-GFP
with AtARF1(T31N)
with AtARF1(Q71L)
with AtSAR1(H74L)
0
20
40
60
80
100
Plastidal / total GFP ratio (%)

Figure 5

Figure 5. Expression and localization of Amyl-1-GFP in onion epidermal cells.

(A) Images of onion epidermal cells expressing Amyl-1-GFP and WxTP-DsRed. Amyl-1-GFP, green (left); WxTP-DsRed, red (middle); GFP and DsRed merged (right), showing that Amyl-1-GFP is co-localized with a plastid stroma marker WxTP-DsRed. Lower panels illustrate a plastid in close-up.
(B) Control experiments. Labeling with WxTP-DsRed and either WxTP-GFP (left), GFP (middle), or AmyII-6-GFP (right) was performed.
(C) Effects of AtARF1(T31N), AtARF1(Q71L) and AtSAR1(H74L) on the targeting of Amyl-1-GFP into plastids visualized with WxTP-DsRed.
In panels **[A]** to **[C]**, twenty to thirty images per cell, from the top to middle of the cell, every 1–2 µm, were taken and combined into one image.
(D) The precise distribution of Amyl-1-GFP and AmyII-6-GFP in onion cells. Upper: Amyl-1-GFP and WxTP-DsRed. Extended focus view constructed from 13 sections spanning the entire plastid, every 0.64 µm. Lower: AmyII-6-GFP and WxTP-DsRed. View constructed from 15 sections, every 0.69 µm.
(E) Statistical evaluation of the plastidial localization of Amyl-1-GFP. Fluorescence ratios were determined of plastidial per sum total of GFP intensity in whole cells. Values show the means ± s.d. (n = 12).

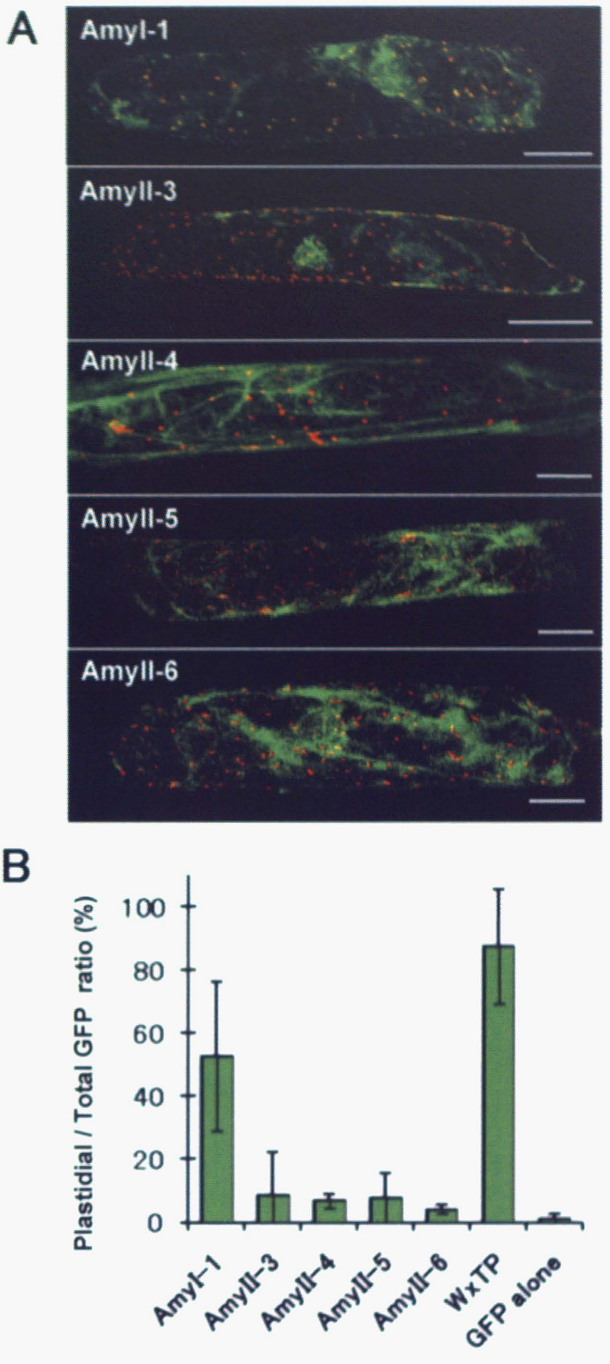

Figure 6. Distinct localization of various Amy isoforms in onion epidermal cells.

(A) Simultaneous expression of WxTP-DsRed and either AmyI-1-, AmyII-3-, AmyII-4-, AmyII-5- or AmyII-6-GFP was carried out. The merged images were constructed as described in Figure 3. Bars represent 100 μm. **(B)** Statistical evaluation of the plastidial localization of different Amy isoforms. Fluorescence ratios were determined of plastidial per sum total of GFP intensity in whole cells. Values show the means ± s.d. (n = 4).

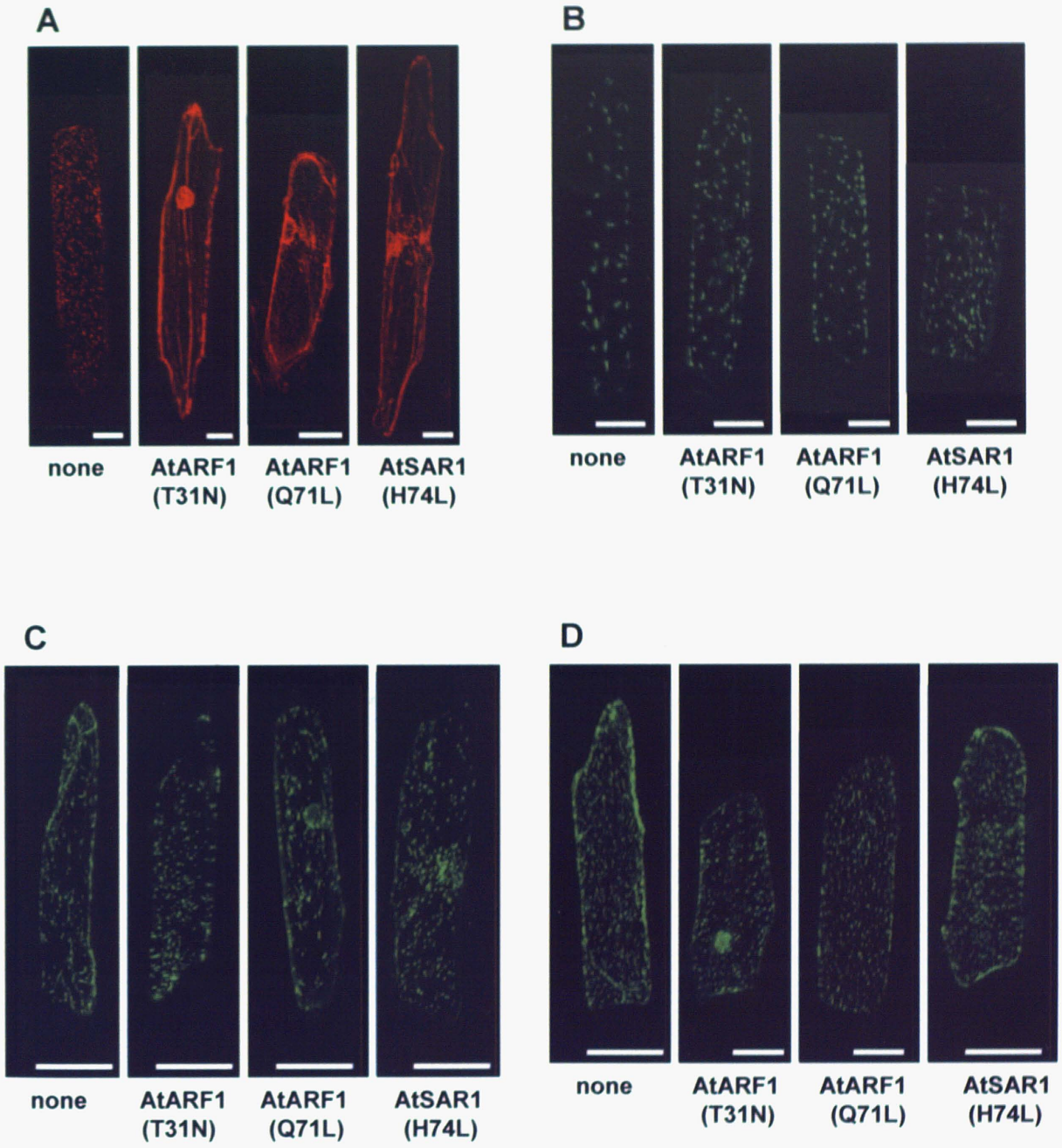
A
none
AtARF1 (T31N)
AtARF1 (Q71L)
AtSAR1 (H74L)
B
none
AtARF1 (T31N)
AtARF1 (Q71L)
AtSAR1 (H74L)
C
none
AtARF1 (T31N)
AtARF1 (Q71L)
AtSAR1 (H74L)
D
none
AtARF1 (T31N)
AtARF1 (Q71L)
AtSAR1 (H74L)

Figure 7

Figure 7. Effects of AtARF1(T31N), AtARF1(Q71L) and AtSAR1(H74L) on the localization of various organelle markers.

Simultaneous expression of the organelle marker and either AtARF1(T31N), AtARF1(Q71L) or AtSAR1(H74L) was carried out in onion cells. **(A)** trans-Golgi marker (ST-mRFP), **(B)** plastidial marker (WxTP-GFP), **(C)** peroxisomal marker (per-GFP), **(D)** mitochondrial marker (mt-GFP). Twenty to thirty images per cell, from the top to middle of the cell, every 1–2 μm, were taken and combined into one image. Bars represent 100 μm.

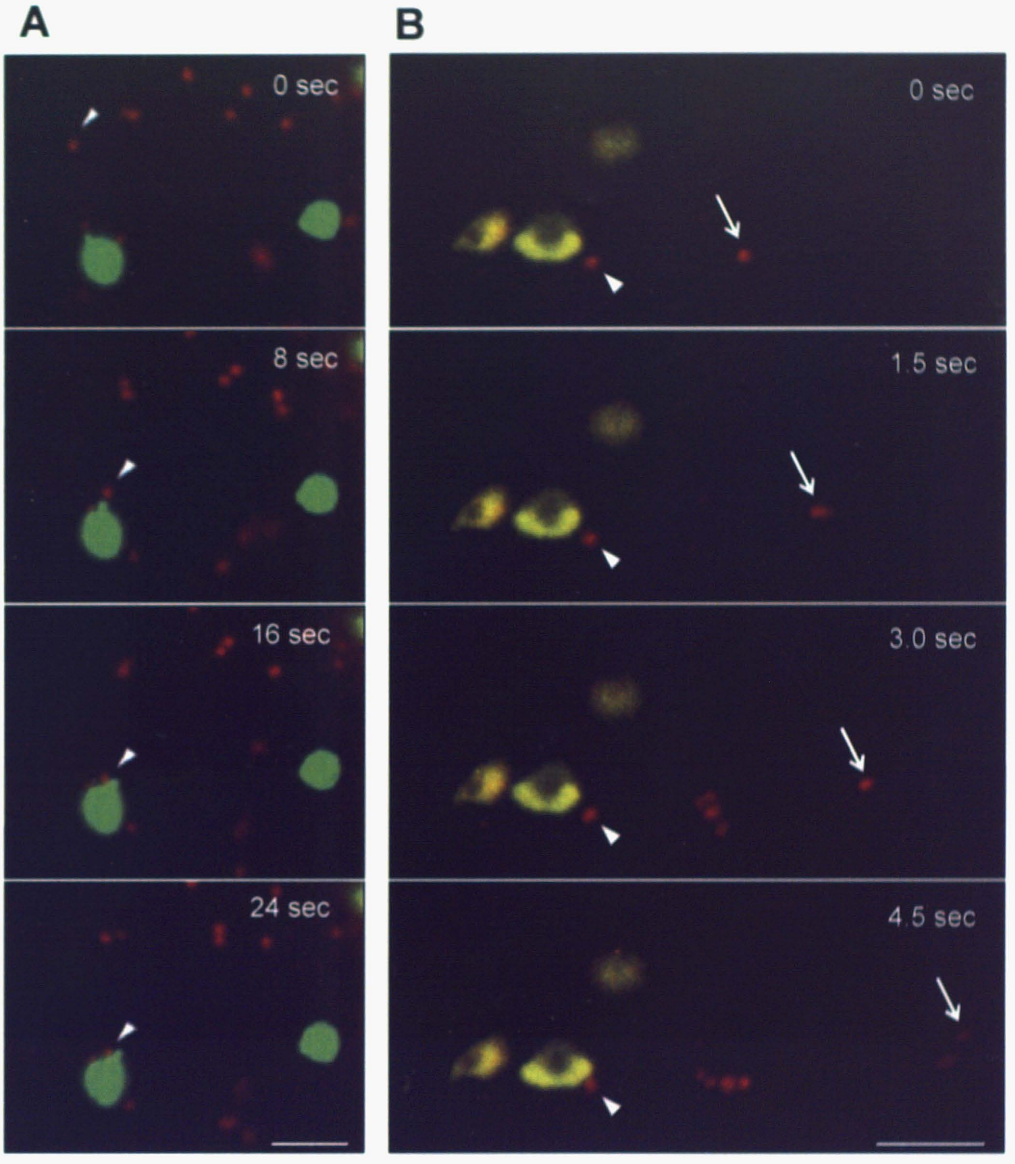

Figure 8

Figure 8. Two-dimensional time-lapse imaging of a communication between Golgi and plastid.

ST-mRFP and WxTP-GFP dual labeling with AmyI-1 expression was carried out in onion cells.
(A) The images were taken at the rate of one frame per 4 sec. Cropped frames from the movie are shown here. Arrowhead shows the Golgi body soft-landing on the surface of the plastid.
(B) The other images were taken at the rate of one frame per 0.5 sec. Cropped frames from the movie are shown here. Arrows show the Golgi bodies having different locomoting characters: one remaining around the plastids (arrowhead) and the other exhibiting active movement (arrow).
ST-mRFP, red; WxTP-GFP, green. Bars represent 5 μm.

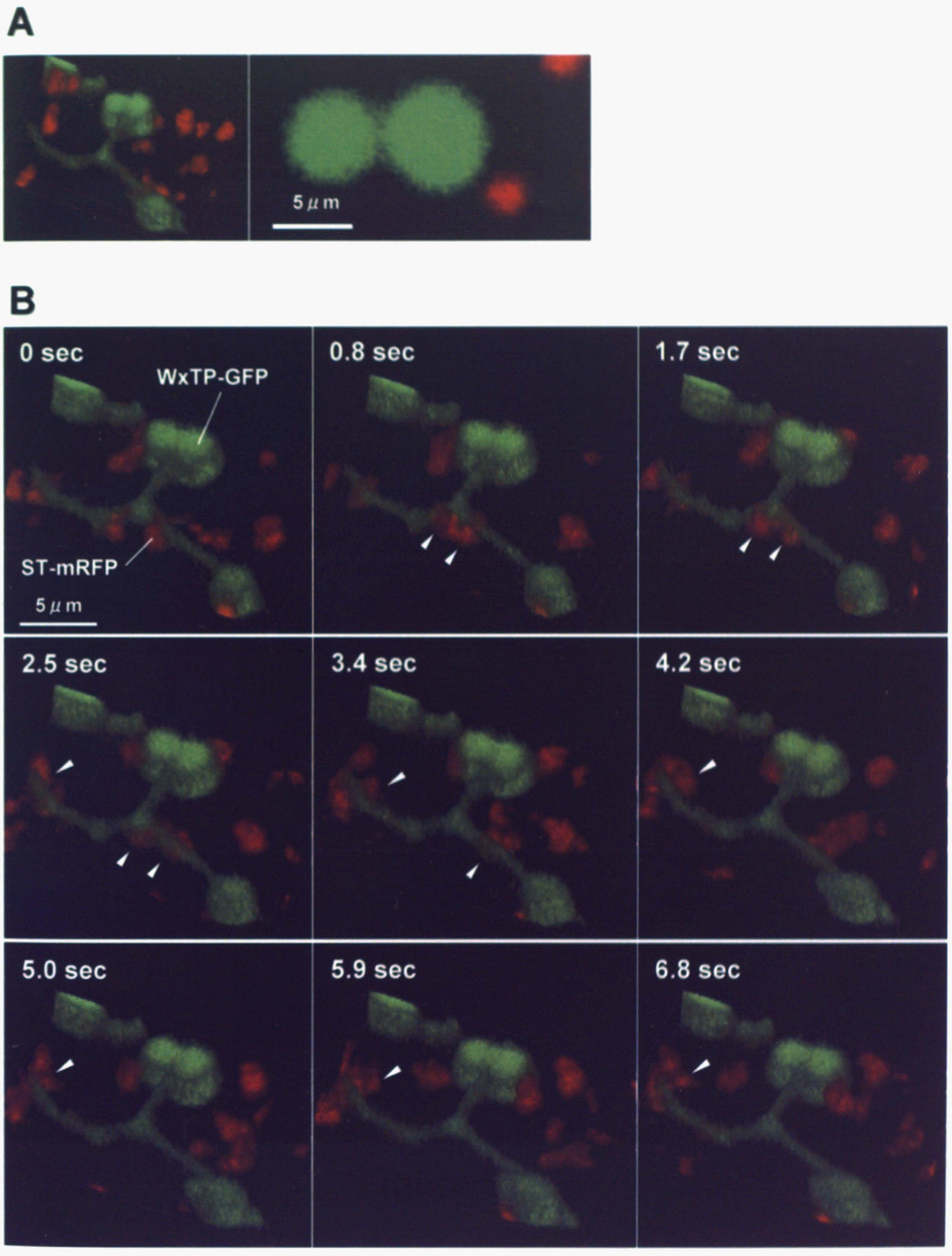
A
5 μm
B
0 sec
WxTP-GFP
ST-mRFP
5 μm
0.8 sec
1.7 sec
2.5 sec
3.4 sec
4.2 sec
5.0 sec
5.9 sec
6.8 sec

Figure 9-1

Figure 9-1 Three-dimensional time-lapse imaging of Golgi-to-plastid traffic.

(A)ST-mRFP and WxTP-GFP labeling without Amyl-1. Left panel represents three-dimensional images reconstructed from ten optical sections spanning the entire plastid, every 1.5 μm. Right panel shows a representative section of a plastid in close-up.
(B) ST-mRFP (red) and WxTP-GFP (green) dual labeling without Amyl-1 expression in onion cells (Three-dimensional time-lapse images). The cells expressing ST-mRFP and WxTP-GFP were observed under a confocal microscope while scanning in the z axis. Ten optical sections, 1.5 μm apart, were taken at 0.844 sec intervals. Three-dimensional time-lapse images were reconstructed using an alpha-blend procedure. The video speed is 4.2-fold of real time. Bar = 5 μm.

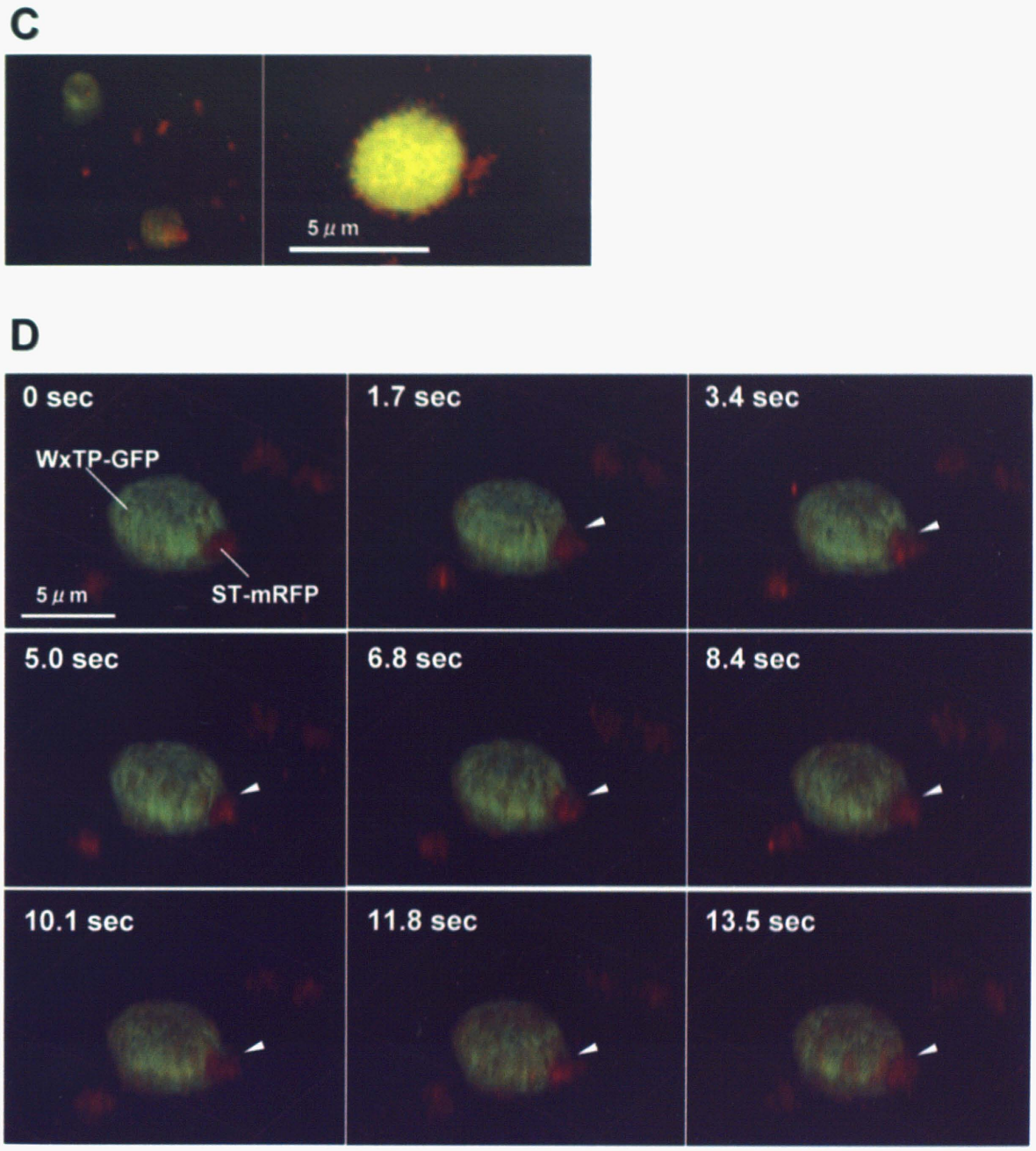
C
5 μm
D
0 sec
WxTP-GFP
5 μm
ST-mRFP
1.7 sec
3.4 sec
5.0 sec
6.8 sec
8.4 sec
10.1 sec
11.8 sec
13.5 sec

Figure 9-2

Figure 9-2 Three-dimensional time-lapse imaging of Golgi-to-plastid traffic.

(C)ST-mRFP and WxTP-GFP labeling with Amyl-1. Left panel represents three-dimensional images reconstructed from ten optical sections spanning the entire plastid, every 1.5 μm. Right panel shows a representative section of a plastid in close-up.
(D) ST-mRFP (red) and WxTP-GFP (green) dual labeling with Amyl-1 expression in onion cells (Three-dimensional time-lapse images). The cells expressing ST-mRFP and WxTP-GFP were observed under a confocal microscope while scanning in the z axis. Ten optical sections, 1.5 μm apart, were taken at 0.844 sec intervals. Three-dimensional time-lapse surface images were reconstructed using an alpha-blend procedure employing Olympus FV10-ASW software. Small membrane vesicles labeled with ST-mRFP were observed on the surface of the plastid. The video speed is 4.2-fold of real time. Bar = 5 μm.

E

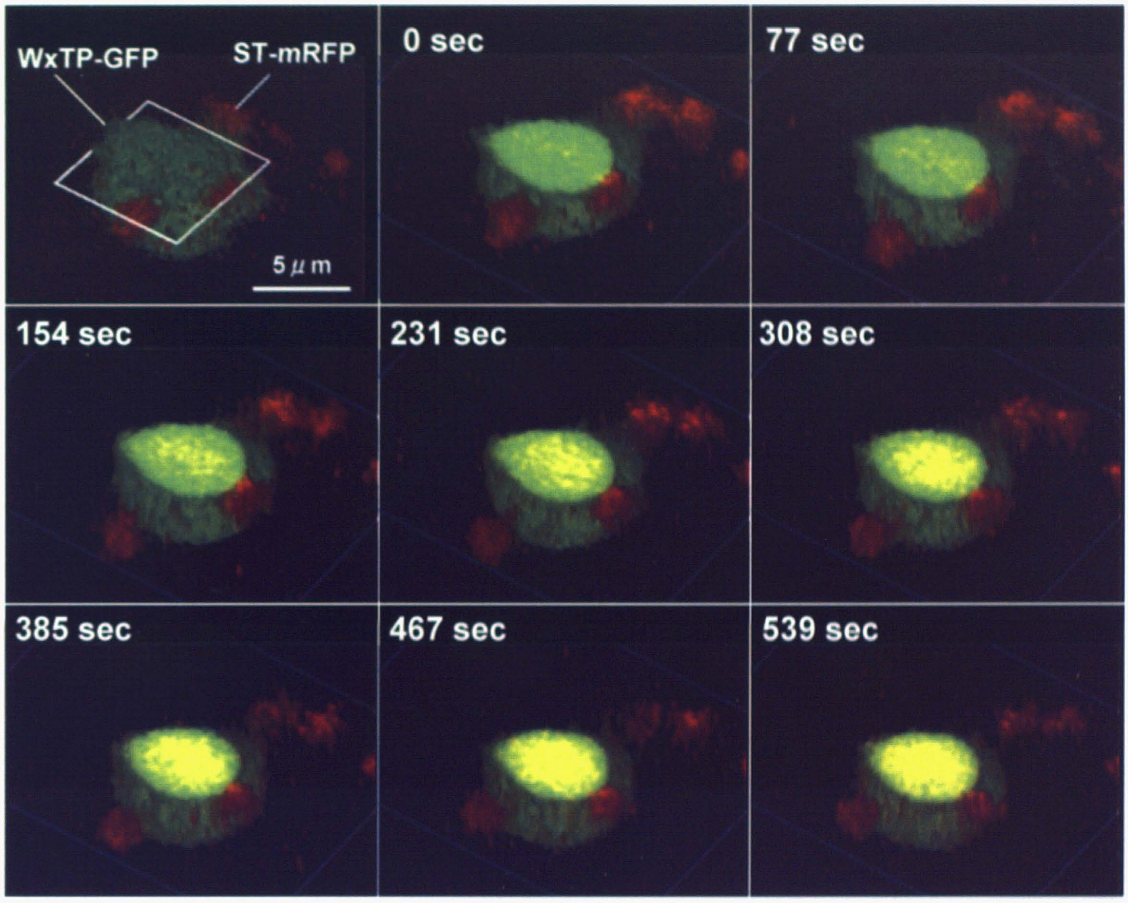
WxTP-GFP
ST-mRFP
5 μm
0 sec
77 sec
154 sec
231 sec
308 sec
385 sec
467 sec
539 sec

Figure 9-3

Figure 9-3 Three-dimensional time-lapse imaging of Golgi-to-plastid traffic.

(E)ST-mRFP (red) and WxTP-GFP (green) dual labeling with Amyl-1 expression in onion cells (Three-dimensional time-lapse images). The cells expressing ST-mRFP and WxTP-GFP were observed under a confocal microscope while scanning in the z axis. Ten optical sections, 1.5 μm apart, were taken at 0.844 sec intervals. Three-dimensional time-lapse images were reconstructed a representative section, the third section from the top that indicated by open blue quadrangle and three-dimensional surface images constructed with sections from No. 4 to 10 using Olympus FV10-ASW software. The ST-mRFP-labeled membrane vesicles were found to be relocated to the interior of the plastid. The video speed is 4.2-fold of real time. Bar = 5 μm.

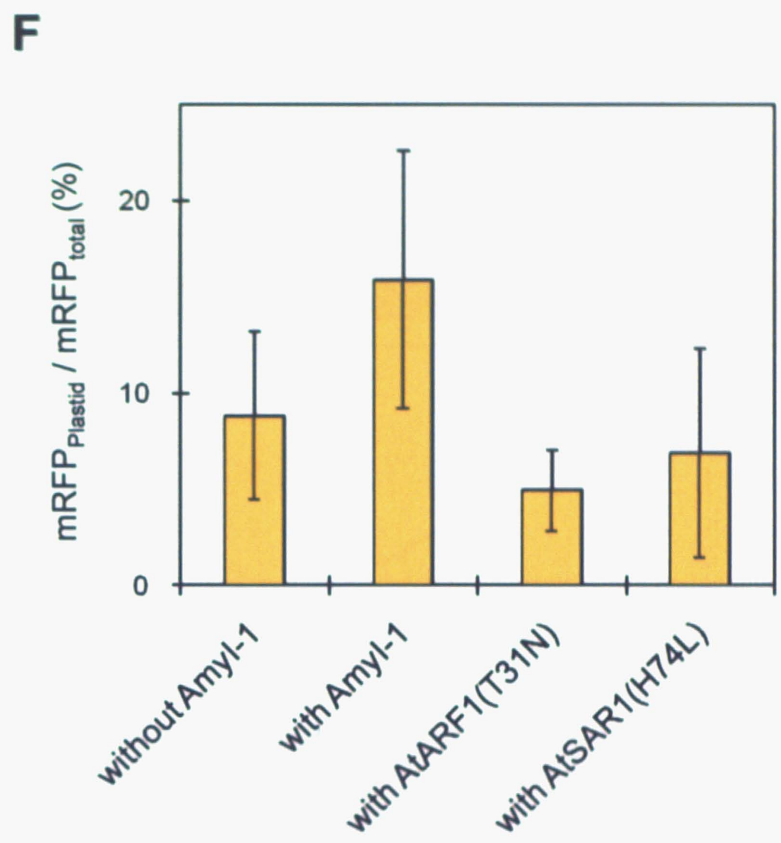

Figure 9-4 Three-dimensional time-lapse imaging of Golgi-to-plastid traffic.

(F) Statistical evaluation of the plastidial localization of ST-mRFP. Fluorescence ratios were determined of plastidial per sum total of RFP intensity in whole cells. Values show the means ± s.d. (*n* = 5-13).

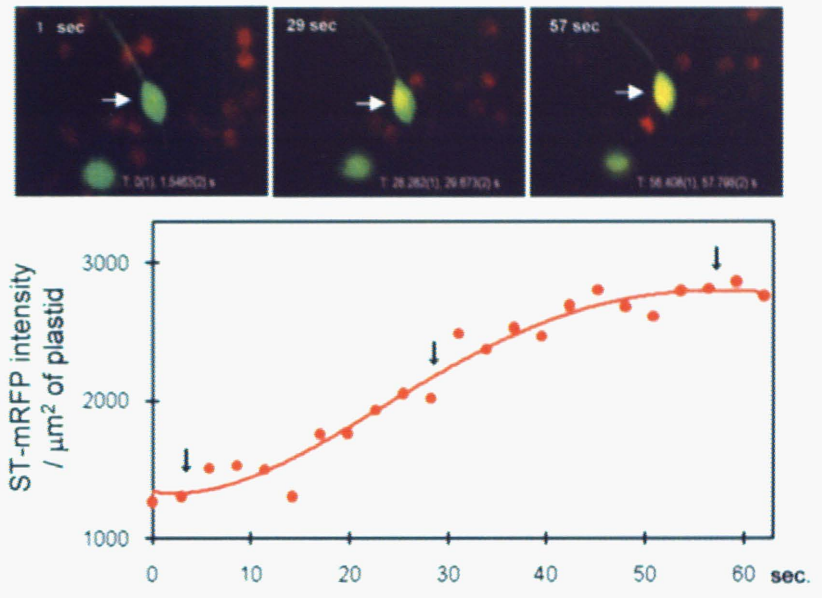

Figure 10. Merging of the trans-Golgi maker into a plastid without Amyl-1 expression.

ST-mRFP and WxTP-GFP dual labeling without Amyl-1 expression was carried out in onion cells. Upper panel: 2D time-lapse scanning. The images were taken at the rate of one frame per 1.156 sec. Three frames at intervals of 28.9 sec are shown here. A representative plastid, indicated by the white arrow, was subjected to quantitative analysis. Lower panel: quantitative evaluation of the plastidial localization of ST-mRFP. Statistical evaluation of the plastidial localization of ST-mRFP. Expression and co-localization of ST-mRFP and WxTP-GFP were determined without or with either Amyl-1, AtARF1(T31N) or AtSAR1(H74L) expression. The intensities of ST-mRFP per μm^2 of plastid were determined and compared.

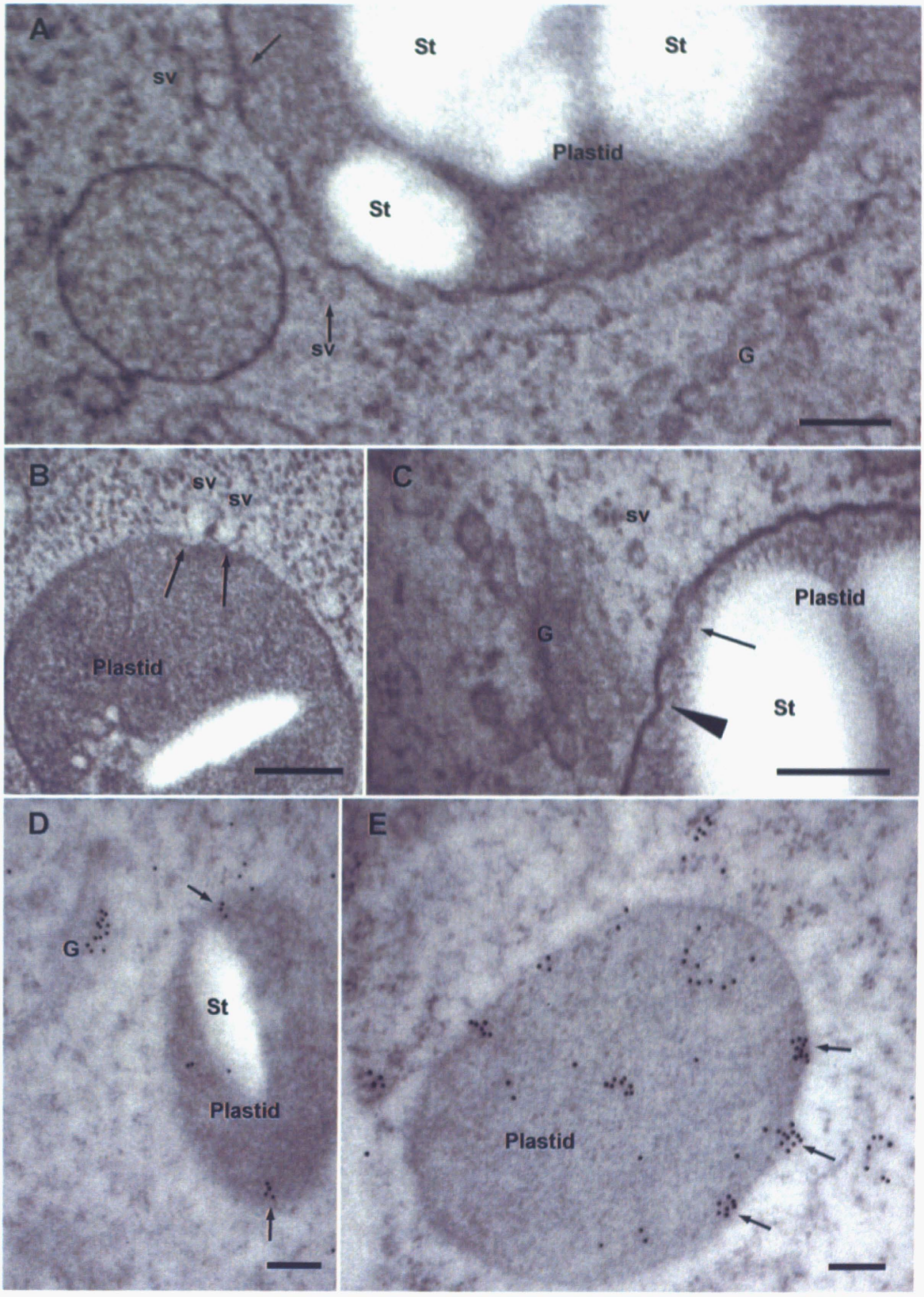
A
sv
St
St
Plastid
St
sv
G
B
sv
sv
Plastid
C
sv
Plastid
G
St
D
G
St
Plastid
E
Plastid

Figure 11

Figure 11. Electron microscopic characterization of Golgi-to-plastid traffic using high-pressure frozen/freeze substituted cells.

Rice cells (A3-1) cultured in MS medium containing 3 % sucrose at 28 °C for 4 days were quickly frozen in a high-pressure freezer.
(A) to (C) Morphological observations. Arrows in **[A]** represent obvious adhesions of membrane vesicles to plastids. In **[B]**, arrows show the moment of plastid entry of membrane vesicles. In **[C]**, a tight association of the Golgi stack to a plastid (arrowhead) and vesicles taken up inside the plastid (arrow) are shown.
(D) and **(E)** Immunocytochemical observations. The ultra-thin sections were labeled with anti-Amyl-1 antibodies and 12-nm colloidal gold particles coupled to goat anti-rabbit IgG. Arrows in **[E]** indicate the clustered Amyl-1 proteins entering the plastid.
G, Golgi; St, starch; sv, small membrane vesicle. Bars represent 200 nm.

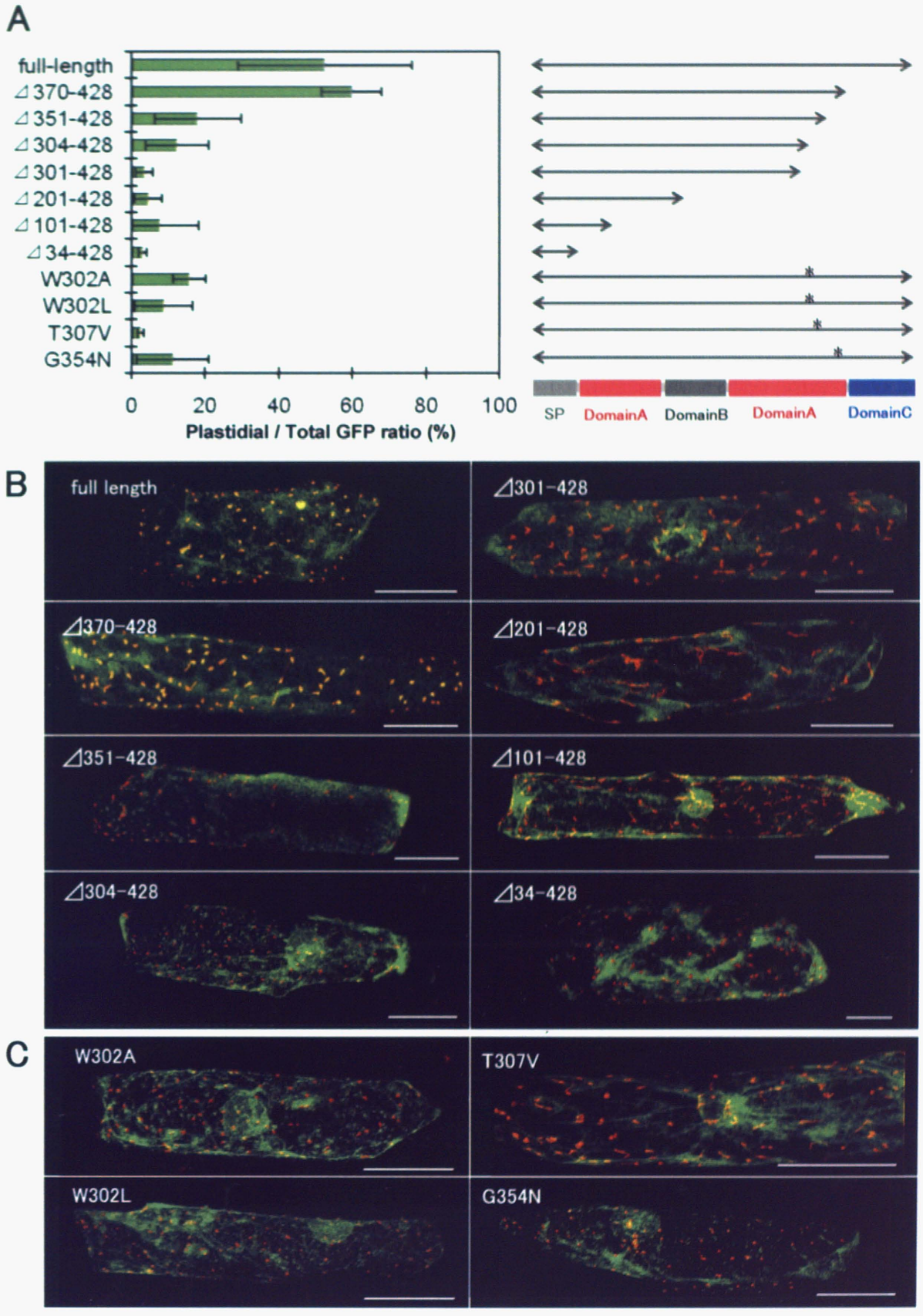
A
full-length
⊿370-428
⊿351-428
⊿304-428
⊿301-428
⊿201-428
⊿101-428
⊿34-428
W302A
W302L
T307V
G354N
0
20
40
60
80
100
Plastidial / Total GFP ratio (%)
SP
DomainA
DomainB
DomainA
DomainC
B
full length
⊿301-428
⊿370-428
⊿201-428
⊿351-428
⊿101-428
⊿304-428
⊿34-428
C
W302A
T307V
W302L
G354N

Figure 12

Figure 12. Evaluation of plastid targeting abilities of various carboxyl-terminal truncated or site-directed mutated Amyl-1.

Simultaneous expression of WxTP-DsRed and a carboxyl-terminal truncated Amyl-1 (either full length, △370–428, △351–428, △304–428, △301–428, △201–428, △101–428 or △34–428) or either Amyl-1(W302A)-, Amyl-1(W302L)-, Amyl-1(T307V)- or Amyl-1(G354N) fused to GFP was carried out in onion cells.
(A) Right: diagram of the Amyl-1 series. Asterisks indicated the substituted residues. ; Left: quantitative results. Fluorescence ratios were determined of plastidial per sum total of GFP intensity in whole cells. Values show the mean ± s.d. obtained in four independent experiments.
(B) (C) Typical images. Bars represent 100 μm.

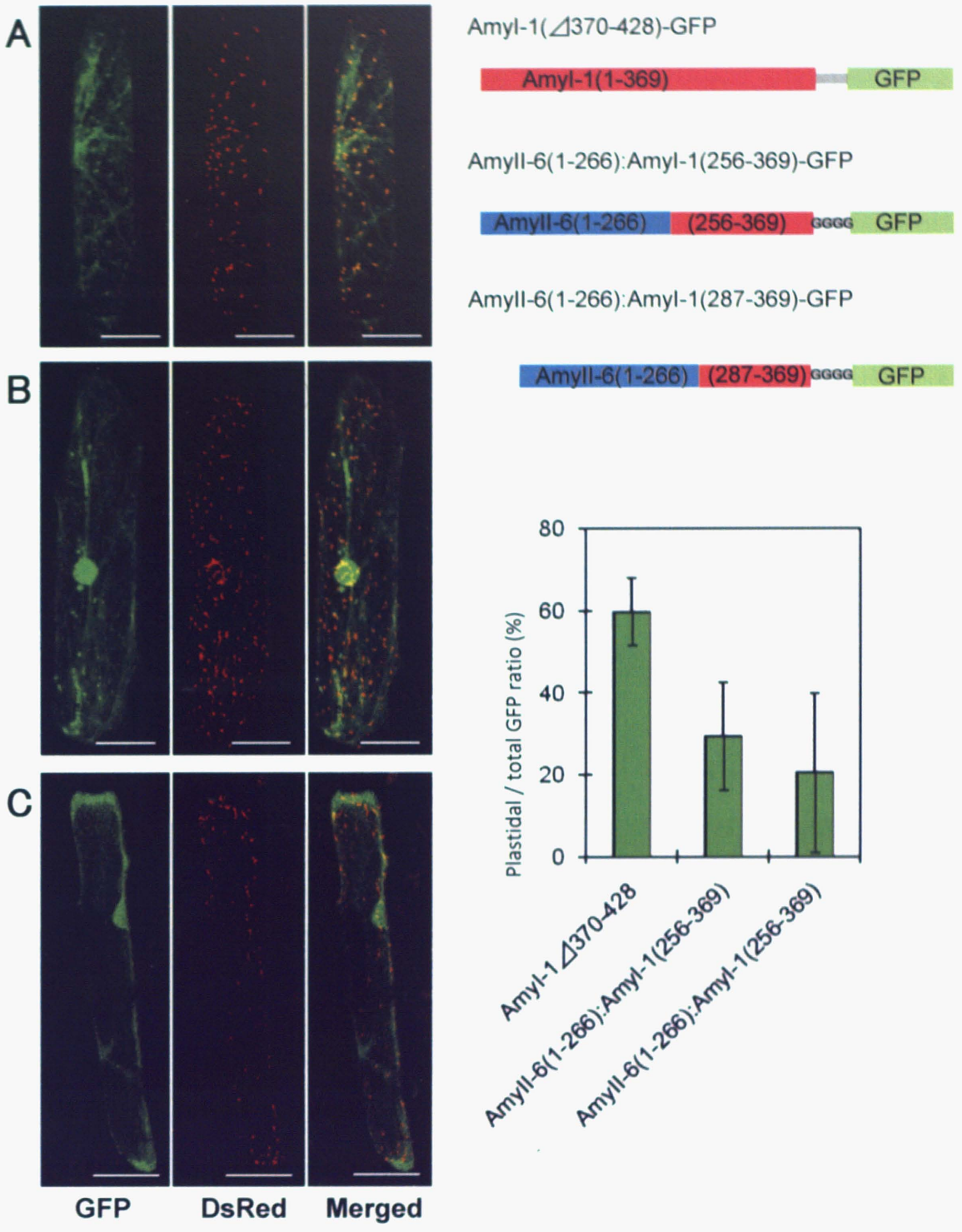

Figure 13. Plastid targeting abilities of AmyII-6:AmyI-1 chimera proteins.

(A) AmyI-1(1-369)-GFP
(B) AmyII-6(1-266):AmyI-1(256-369)-GFP
(C) AmyII-6(1-266):AmyI-1(287-369)-GFP
The AmyII-6:AmyI-1 chimera proteins showed little targeting to the plastids visualized with WxTP-DsRed in onion cells. The merged images were constructed as described in Figure 3.
Bars represent 100 mm.

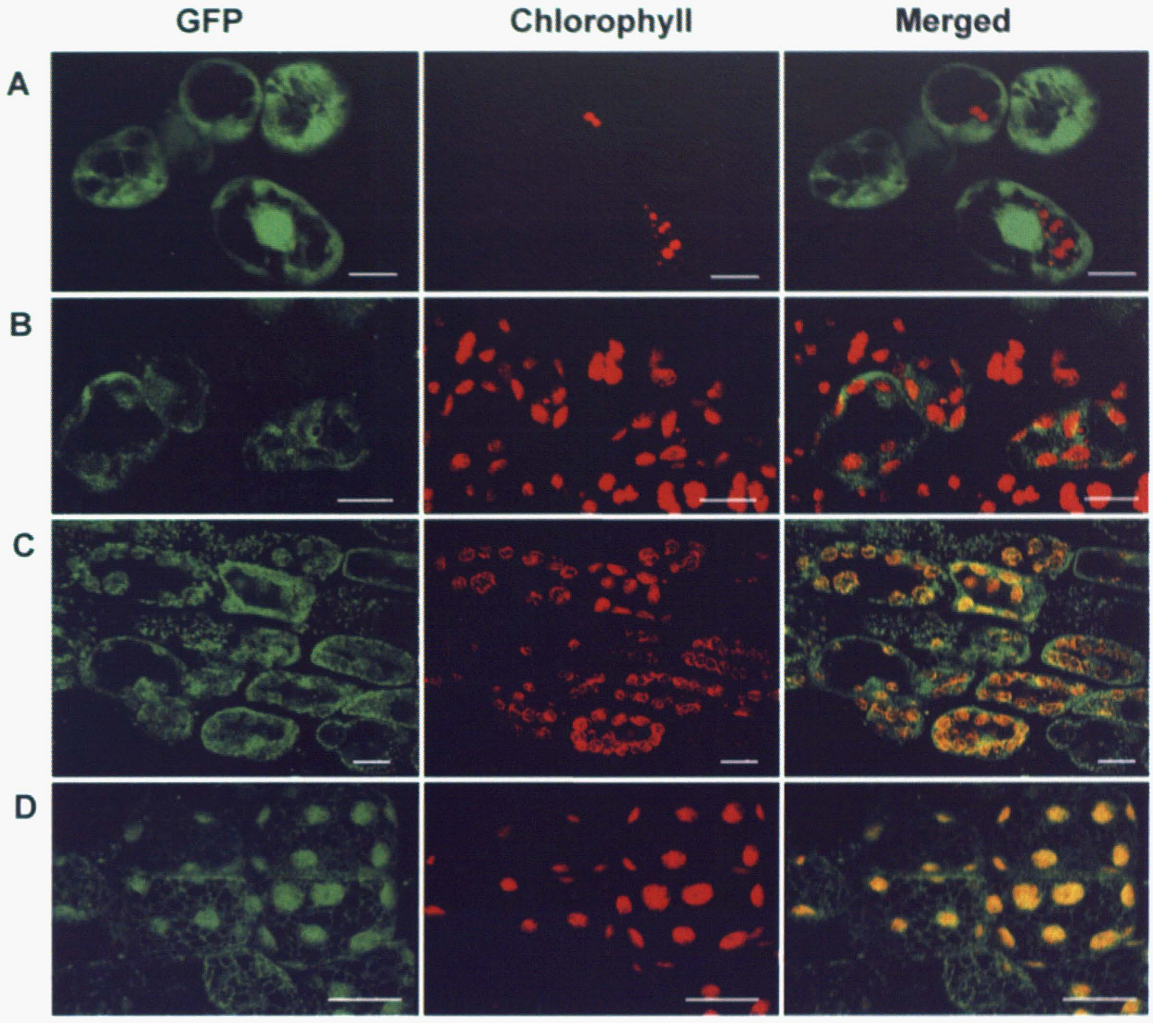

Figure 14

Figure 14. Fluorescence images in green cells of transgenic rice transformed with *Amyl-1(△101–428)–GFP.*

The stable transformant cells were sectioned with a vibratome to 25 μm thickness, and immediately observed by means of confocal laser scanning microscopy. **(A)** GFP alone, **(B)** Amyl-1(△101–428)–GFP, **(C)** Amyl-1 (△370–428)–GFP and **(D)** Amyl-1-GFP. Left, GFP fluorescence; middle, chlorophyll autofluorescence; right, merged image. Bars represent 5 μm.

DISCUSSION

AmyI-1 degrades starch granules in living rice cells

It is widely accepted that α-amylase plays the most important role in starch breakdown in germinating cereal seeds. This enzyme is excreted from the secretory tissues to the storage tissue, in which the starch granules are bared. However, recent investigations have also revealed the involvement of α-amylase in starch degradation in living rice cells (Chen et al., 1994; Asatsuma et al., 2005). Immnocytochemical studies have shown that α-amylases are localized in multiple compartments, such as amyloplasts, vacuoles and cell walls (Chen et al., 1994). Moreover, a rice α-amylase isoform, αAmy3, occurred in the chloroplasts of transgenic tobacco leaves (Chen et al., 2004). Transgenic rice plants that overexpressed α-amylases produced white immature seeds that show reduced starch accumulation (Asatsuma et al., 2006). The present study provides further evidence that the AmyI-1 glycoprotein is localized in the amyloplasts and degrades starch granules within the organelles in rice callus cells (Figure 2). Thus, rice α-amylase exhibits dual targeting to endomembranes/extracellular spaces and plastids (Chen et al., 2004). Protein import to plastids through a secretory pathway does not fit in with the traditional cell biological context and appears to be an inelegant system compared with the canonical plastid import machinery. However, the chloroplast targeting of α-amylase in leaf cells is physiologically relevant, since starch turnover in chloroplasts is a crucial process in leaves, and no starch is present outside of the cells. The plastid targeting route from the endomembrane system appears to be operated as a physiological event in plants.

AmyI-1 contains a plastid-targeting signal common to both rice and onion cells

Several α-amylase isoforms, such as AmyI-1 (*RAmy1A, αAmy7*), II-3 (*RAmy3E, αAmy8*) and II-4 (*RAmy3D, αAmy3*) have been shown to occur within the plastids in rice cells (Chen et al., 2004; Asatsuma et al., 2005). However, only AmyI-1 exhibited clear and efficient targeting into the plastids in the onion epidermal cells. AmyII-3 and AmyII-4 were rarely transported to the plastids (Figure 5 and Figure 6). AmyI-1's plastid-targeting signal thus functions in both rice and onion cells. Plastid-targeting signals of two other isoforms are considered to be insufficient in the context of the onion system. Yu and colleagues have revealed, employing a series of loss-of-function and gain-of-function analyses, that the ER signal peptides of αAmy3 and αAmy8 direct cargo proteins to plastids and extracellular compartments in rice and tobacco cells (Chen et al., 2004). In contrast, the signal peptide of AmyI-1 failed to deliver reporter protein GFP to plastids in onion cells and chloroplasts in rice green cells (Figure 12 and Figure 14). I believe that the AmyI-1 signal peptide contains no information for directing cargo protein, including its own structural protein, to the plastids. The divergence in roles of the signal peptides of rice α-amylases remains unresolved.

Golgi-to-plastid traffic

Intracellular compartments in eukaryotic cells can be divided into at least five distinct families. The first and second compartments are the cytosol and the nucleus. The third includes all single-membrane organelles that function in the secretory and endocytic pathways, and possibly microbodies (peroxisomes). The fourth and fifth are mitochondria and plastids: the latter includes chloroplasts in green leaves and amyloplasts in starchy cells. The lumen of the ER, the Golgi apparatus, and lysosomes or vacuoles, are topologically equivalent to the extracellular space, and the membranes of the organelles, collectively called endomembrane organelles, may have evolved from the plasma membrane. Cycles of membrane budding and fusion permit communication with the endomembrane and cell exterior via transport vesicles (Rothman and Wieland, 1996). It has been long accepted that mitochondria and plastids are isolated from the traffic between organelles in the third compartment group (Blobel, 1980). However, communications between the intracellular compartments in higher plant cells are much more flexible than previously thought. In the present study, I demonstrated that the Golgi stacks were tightly associated with the plastids (Figure 11C), and that a Golgi-resident protein, ST-mRFP, was actually incorporated into the interior of the plastid (Figure 9E), indicating the existence of a protein traffic route from the Golgi complex to plastids. In addition, the incorporation of Golgi-resident proteins into plastids was stimulated by AmyI-1 expression (Figure 9F), and the plastid-targeting of both AmyI-1 and ST-mRFP was similarly inhibited by arresting the ER-to-Golgi traffic (Figures 5E and 9F). Thus, the Golgi apparatus appears to directly communicate with plastids to import glycoprotein cargo into this organelle.

In *Euglena,* a fusion event of the Golgi-derived vesicles to the outermost of the three chloroplast envelope membranes has been observed (van Dooren et al., 2001). It is a potential candidate for the import mechanism of glycoproteins into plastids in higher plant cells. In this model, however, two puzzling problems must be resolved: one is the topology of the targeted space and the other is the recycling of fused membranes. Membrane fusion between the Golgi-derived vesicles and the outer envelope of plastids would result in localization of the cargo in the intermembrane space between the outer and inner envelopes. It has recently been proposed that three routes may operate for transfer from the intermembrane space to the stroma after delivering cargo materials to the space: (a) engagement of an unknown transporter in the inner envelope membrane; (b) passage through the Tic transporter operating independently of the Toc machinery; or (c) vesicle budding from the inner membrane itself (Radhamony and Theg, 2006). My present study strongly supports vesicle-mediated import of the AmyI-1 glycoprotein into plastids. EM observations have shown that the Golgi-derived vesicles bind physically to plastids, and the clustered AmyI-1 proteins appeared to pass through the envelope membranes and enter the stromal space (Figure 11). However, it should be noted that AmyI-1 importation does not take place by means of the simple membrane fusion described in the *Euglena* model. Three-dimensional time-lapse imaging shows that the trans-Golgi membranes appear to be taken up and spread inside the plastid (Figure 9E). In addition, the moment of plastid entry of membrane vesicles was seen in EM observations using quick-frozen cells (Figure 11A and B): the vesicles might pass through the plastid envelope membranes other than by microautophagy-like invagination into the organelle. If microautophagy-like invagination were involved in the uptake of membrane vesicles, vesicles encircled by the plastid envelope membranes

in addition to its invagination would be frequently detected in the stroma. However, distinctive vesicles such as these were extremely rare, suggesting that an unresolved vesicle uptake mechanism operates in AmyI-1 importation into plastids. The imported vesicles are perhaps subsequently broken up in the organelle.

The Golgi apparatus is known to be a multifunctional organelle, responsible for the biosynthesis of cell wall polysaccharides, the processing and modification of glycoproteins, and the sorting of polysaccharides and proteins destined for different locations (Staehelin and Moore, 1995). During the mitosis of tobacco BY-2 cells, about 20% of the Golgi bodies remain close to the spindle, whereas another 20% relocate to the equatorial region near the plasma membrane. These regions are devoid of mitochondria and plastids (Nebenführ et al., 2000). My results revealed that the Golgi bodies in onion cells have at least two different locomoting characters. One group stayed around the plastids, while the other exhibited active movement (Figure 8B). Thus, the localization of Golgi bodies in the cells depends upon their environmental and functional situations. Recent investigations have demonstrated that Golgi stacks are *de novo* constructed and mature in yeast (Matsuura-Tokita et al., 2006), and the rate of cisternal maturation is rapid, matching the rate of protein transport through the secretory pathway (Losev et al., 2006). It is conceivable that Golgi bodies destined for plastid delivery are also newly formed for appropriate situations.

Characterization of the plastid-targeting signal of AmyI-1

Secretion is thought to be a default targeting pathway in both plant and animal cells: that is, in the absence of any other sorting information within the protein, it travels through the ER and Golgi network, and is finally liberated from the cells. Plastidial glycoproteins may possess certain targeting signals for their localization; however, no details of plastid-targeting signals have so far been revealed. The present study demonstrated that the plastid-targeting signal of AmyI-1 is embedded in the protein structure of the enzyme. The results obtained by site-directed mutations of Trp^{302} and Gly^{354}, located on the surfaces of opposite sides of the AmyI-1 protein, suggest that multiple surface regions are necessary for plastid targeting (Figure 12). There was no sequence resemblance among the three glycoproteins (AmyI-1, NPP1 and CAH1) shown to occur in plastids. We thus infer that the plastid-targeting signals of glycoproteins are expressed by as yet uncharacterized three-dimensional structures.

Vacuolar proteins are synthesized and translocated into the ER lumen, then delivered to the vacuole through the secretory pathway. The sorting of vacuolar proteins requires interaction between the protein's sorting signal and a sorting receptor within the endomembranes (Kirsch et al., 1996; Matsuoka and Neuhaus, 1999; Vitale and Hinz, 2005; Fuji et al., 2007). Vacuolar sorting signals are grouped into three categories: sequence-specific signals, C-terminal signals, and physical structure signals (Vitale and Hinz, 2005). Three vacuolar proteins have been reported to possess physical structure vacuolar sorting signals (Saalbach et al., 1991; von Schaewen and Chrispeels, 1993; Törmäkangas et al., 2001). One of these, barley aspartic protease (phytepsin) was shown to reach the vacuoles through the Golgi apparatus in a COPII-mediated manner. A plant-specific insert (PSI) of 104 amino acids present in the phytepsin serves as a

vacuolar sorting signal. Deletion of the PSI causes efficient secretion of Phytepsin PSI in a COPII-independent manner. I observed that the dominant negative and constitutive active mutants of ARF1 and SAR1 effectively prevent the targeting of AmyI-1 into the plastids and keep them in the ER in onion epidermal cells (Figure 5C), indicating that the plastid targeting of AmyI-1 requires COP-mediated membrane traffic. It is apparent that the ER-Golgi system, located in the early secretory pathway, acts as a set of sorting stations for delivering proteins to the plastids in addition to the vacuoles. However, the molecular machinery that recognizes these physical targeting signals remains unknown.

Based on our overall results, I propose a model for glycoprotein-targeting plastids in higher plant cells (Model-2). The plastidial glycoprotein is synthesized in the ER and transported to the Golgi in a way that is dependent on ARF1 and SAR1 GTPases. A physical structure signal for their plastid targeting is recognized by hypothetical receptor(s) placed on the early secretory pathway. Golgi bodies with cargo, which are specialized for delivering a glycoprotein cargo to the plastids, might move to the plastid in a targeting signal-dependent manner, after which small membrane vesicles derived from the Golgi adhere to the plastid's envelope membrane. The imported vesicles are eventually broken up within the plastid stroma, allowing the liberated glycoproteins to function inside the organelle.

Future prospects

In this study, I reported a unique transport system involved in the plastidial targeting of the AmyI-1 glycoprotein and showed that AmyI-1 contains plastid targeting signal common to rice and onion (*Allium cepa*) cells. The plastidial glycoprotein is synthesized in the ER and transported to the Golgi in a way that is dependent on ARF1 and SAR1 GTPases. I proposed a model for glycoprotein-targeting plastids in higher plant cells, however, very little is known about the molecular machinery for importing of glycoprotein into plastids.

To clarify the targeting mechanism of plastidial glycoprotein, it is important that what recognizes targeting signals of plastidial glycoproteins and/or the vesicles from Golgi bodies specialized for delivering glycoprotein cargo to plastids and which steps on the pathway plastid targeting signals were recognized. Two investigations are needed to clarify the targeting mechanism. One is the identification of the physical structure signal for plastid targeting of AmyI-1 and the other is the identification of hypothetical receptor(s) and/or translocon components that recognizes targeting signals of plastidial glycoproteins. Unfortunately crystal structure of AmyI-1 is still unclear. Crystal structure of targeting signal of AmyI-1 will provide information on how the physical structure signal works. I hope that the difference between structures of native AmyI-1 and site-directed mutated AmyI-1 is clarified. Furthermore, identification of receptor(s) that recognizes targeting signals of AmyI-1 is necessary. Is physical targeting signal of AmyI-1 recognized by the receptor located on ER? Or, are plastidial glycoproteins transported into Golgi bodies as cargo, which are specialized for delivering glycoprotein cargo to plastids? Recent evidence showed that inhibition of Golgi function causes plastid starch accumulation (Hummel, et al., 2010). This evidence agrees with my

targeting model and indicates the importance of the Golgi body for plastid targeting of glycoproteins. It is also an interesting topic that the Golgi body specializes for delivering glycoprotein cargo to plastids. A hypothetical signal may change the function of Golgi body through the maturation of Golgi body, which contained in the vesicles from ER.

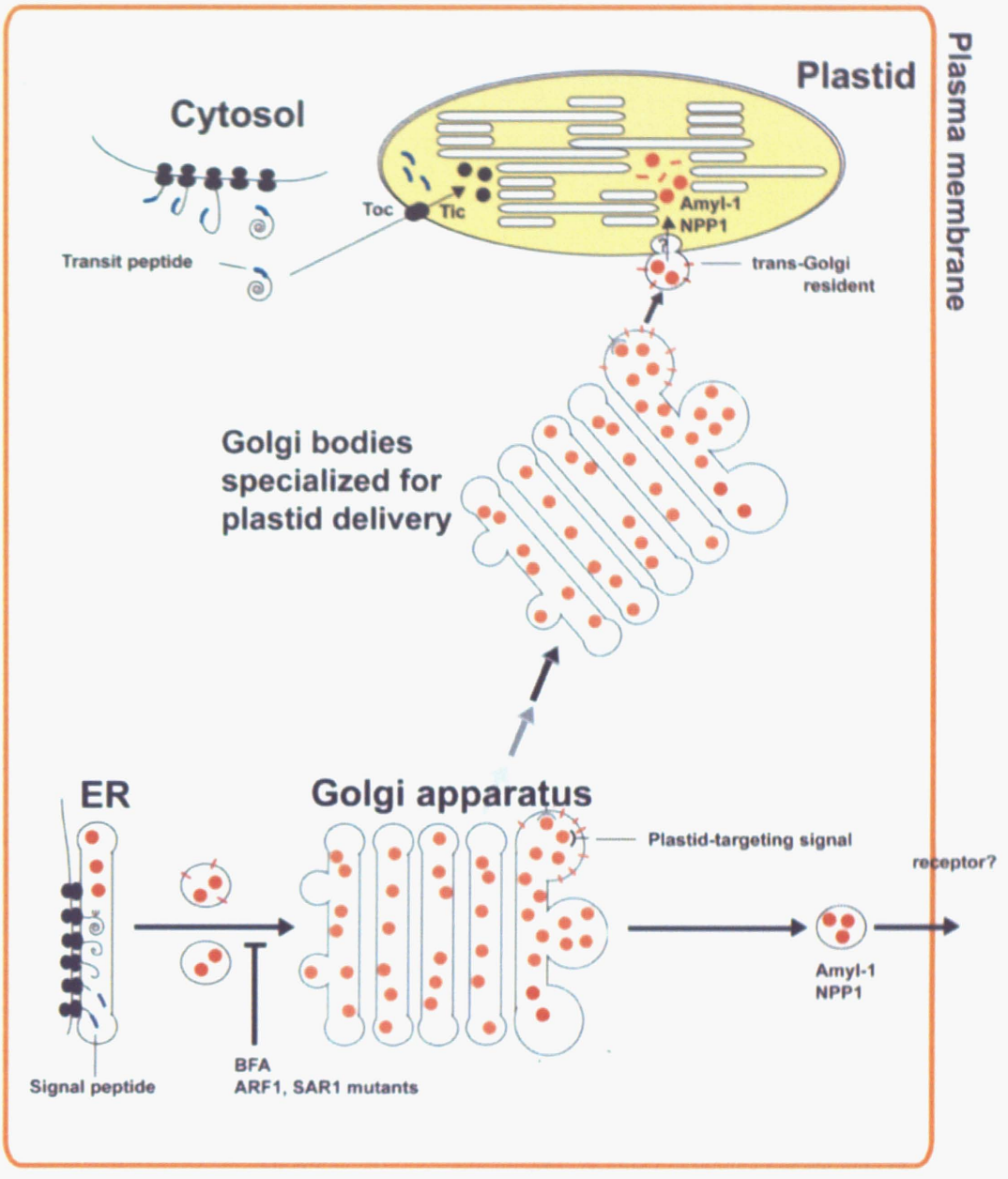

Model-2. A hypothetical model for plastid targeting of glycoproteins from the Golgi apparatus through the secretory pathway.

The plastid-destined glycoproteins such as Amyl-1 and NPP1 are synthesized in the ER lumen and transported to the Golgi apparatus. Plastid targeting of glycoproteins is prevented by the drug BFA and/or the mutants of ARF1 and SAR1, indicating that membrane trafficking is essential to their plastid targeting. The Golgi bodies with cargo, which are specialized for delivering to the plastids, might move to the plastid in targeting signal-dependent manner, after which small membrane vesicles derived from the Golgi adhere to the envelope membrane of the plastid. Both the membrane component and glycoprotein cargo are eventually imported into the interior of plastid through the envelope membranes via an as yet unknown translocating machinery.

SUMMARY

Rice α-amylase isoform I-1 (AmyI-1), well-characterized secretory *N*-linked glycoprotein, was localized within the plastids, and proved to be involved in the degradation of starch granules in the organelles of rice cells. AmyI-1 is synthesized on endoplasmic reticulum (ER)-membrane-bound ribosomes, signal-sequence-dependent translocation of the ER, vesicular transport to the Golgi apparatus, oligosaccharide modification to the complex type, and exocytosis, all proceed according to the canonical secretory mechanism.

Nuclear-encoded plastidial proteins are normally synthesized in the cytosol and post-translationally imported into the organelle. In most cases, precursor proteins are synthesized with an N-terminal pre-sequence called a transit peptide. The transit peptide is necessary for and also sufficient for plastidial targeting and translocation initiation. The transit peptide is recognized by Toc (translocon at the outer envelope of chloroplast) complex and Tic (translocon at the inner envelope of chloroplast) complex. A few plastidial glycoproteins have been reported, however, the mechanism of targeting to plastids.

The aim of this research is to clarify the mechanism of a unique transport system involved in the plastid-targeting of rice AmyI-1 glycoprotein.

The contents are as follows.

AmyI-1 degrades starch granules in living rice cells

In electron microscopic analysis, the amyloplasts of transgenic rice callus cells with constitutively high expression of AmyI-1 had slim starch granules with large interspaces in contrast to the presence of ripe starch granules in the amyloplasts of wild-type cells. Additionally, quantitative measurements showed that the starch content in the callus cells overexpressing AmyI-1 was reduced to approximately half of that in the wild type.

These date showed that AmyI-1 degrade starch granules in living rice cells.

AmyI-1 contains a plastid-targeting signal common to both rice and onion cells

To characterize the nature of plastid localization of AmyI-1 in details, I performed transient expression of α-amylase isoforms (I-1, II-3, II-4, II-5 and II-6) fused with green fluorescent protein (GFP) using onion epidermal cells. AmyI-1-GFP fluorescence overlapped with the plastids visualized by WxTP-DsRed but unlike in the AmyI-1-GFP, the fluorescence of AmyII-3-, AmyII-4-, AmyII-5- and AmyII-6-GFP rarely merged with the plastid marker

These results indicate that AmyI-1, but no other isoforms, possesses a plastid-targeting signal common to both rice and onion cells.

Membrane trafficking is necessary for plastid targeting of AmyI-1

Expression of dominant negative or constitutive active mutants of ARF1 and SAR1, which are defective in GTPase cycling, inhibits the ER-to-Golgi traffic. The transport of AmyI-1-GFP into plastids was severely inhibited by the ARF1 and SAR1 mutants and the fluorescent proteins remained.

These results strongly suggest that the membrane trafficking from the ER is necessary for the plastid targeting of these glycoproteins.

Golgi-to-plastid traffic

In contrast to mammalian Golgi apparatus, plant Golgi stacks show active and "stop-and-go" tumbling movements along actin microfilaments. The active and "stop-and-go" tumbling movement of Golgi stacks suggests that the Golgi stack itself serves as a cargo container.

High-speed two-dimensional and three-dimensional time-lapse analyses using confocal laser scanning microscopy were performed. When ST-mRFP *trans*-Golgi marker and WxTP-GFP plastid marker were simultaneously expressed together with AmyI-1, which would activate Golgi-to-plastid traffic in onion cells, significant merging of ST-mRFP with the GFP-labeled plastids was observed. Moreover, close contact between the two organelles was occasionally observed. Three-dimensional time-lapse imaging showed that even without AmyI-1 expression, the ST-mRFP-labeled Golgi adheres to the surface of plastids and stromules. The incorporation of ST-mRFP into plastids still occurred, albeit at lower frequency. In addition to these, Golgi-to-plastid trafficking was noticeably prevented by the expression of either AtARF1(T31N) or AtSAR1(Q74L).

Electron microscopic studies were carried out of suspension-cultured cells derived from transgenic rice seed (A3-1 line) with a constitutively high expression of AmyI-1 using high-pressure frozen/freeze-substituted techniques. In the electron microscopic images, it was frequently observed that small membrane vesicles, perhaps derived from the Golgi apparatus stayed by their side, adhered to the envelope membrane of plastids. Tight association of the Golgi stacks with the envelope membrane was also observed in the same cells. Furthermore, immunological staining of ultrathin sections with anti-AmyI-1 antibodies revealed the presence of AmyI-1 in both the Golgi apparatus

and the plastids.

Taken together, I strongly inferred that Golgi-to-plastid basal communication occurs under tranquil physiological conditions, and that the AmyI-1 co-expression enhances the flow of Golgi-to-plastid traffic and activates the communication between two organelles in the cell.

Characterization of the plastid-targeting signal of AmyI-1

To identify the plastid-targeting signal of AmyI-1, the transient expression and localization of a series of carboxyl-terminal truncated AmyI-1-GFP fusion proteins was examined in bombarded onion cells. And that indicated the importance of the peptide region from Trp^{301} to Gln^{369} for plastid targeting of AmyI-1.

I selected Trp^{302}, Thr^{307} and Gly^{354}, unique amino acid residues in the region from 301 to 369, for the next site-directed mutagenesis experiments. The substitution of Ala or Leu for Trp^{302} strongly arrested the targeting of AmyI-1-GFP into the plastids. The substitution of Val for Thr^{307} or Asn for Gly^{354} also arrested the plastid targeting of AmyI-1-GFP, as in the W302A and W302L mutations. Furthermore, the chimera proteins of AmyII-6(1-266):AmyI-1(256-369) and AmyII-6(1-266):AmyI-1(287-369) failed to localize in the plastids.

These results indicate that conformational changes in the region from Trp^{301} to Gln^{369} influence the targeting ability.

ACKNOWLEDGEMENTS

I wish to thank Professor Toshiaki Mitsui, Professor Hidetaka Hori, Associate Professor Kimiko Itoh (Niigata-University School of Science and Technology) for their constant guidance, support and suggestions through this study.

I also wish to thank Dr. A. Kato (Niigata University, Japan), Dr. Y. Niwa (University of Shizuoka, Japan), Dr. I. Hwang (Pohang University of Science and Technology, Korea), Dr. R. Tsien (University of California, San Diego, USA) for providing pper-GFP, pmt-GFP, ST and mRFP, Dr. Susan T. Hamamoto (University of California, Berkeley, USA) for tannic acid, Dr. Y. Hayashi (Niigata University, Japan), Yumi Goto and Mayuko Sato (Plant Science Center, RIKEN) for their valued contributions to the EM study. I also thank Miyuki Koumura (Olympus, Tokyo, Japan) for technical support with confocal laser scanning microscopy.

REFERENCES

Asatsuma, S., Sawada, C., Itoh, K., Okito, M., Kitajima, A., and Mitsui, T. (2005). Involvement of α-amylase I-1 in starch degradation in rice chloroplasts. *Plant Cell Physiol.* 46: 858–869.

Asatsuma, S., Sawada, C., Kitajima, A., Asakura, T., and Mitsui, T. (2006). α-Amylase affects starch accumulation in the rice grain. *J. Appl. Glycosci.* 53: 187–192.

Bennett-Lovsey, R.M., Herbert, A.D., Sternberg, M.J., and Kelley, L.A. (2008). Exploring the extremes of sequence/structure space with ensemble fold recognition in the program *Phyre. Proteins* 70: 611–625.

Blobel, G. (1980). Intracellular protein topogenesis. Proc. Natl. Acad. Sci. USA 77: 1496–1500. Bruce, B.D. (2000). Chloroplast transit peptides: Structure, function and evolution. *Trends Cell Biol.* 10: 440–447.

Chen, M.H., Huang, L.F., Li, H.M., Chen, Y.R., and Yu, S.M. (2004). Signal peptide-dependent targeting of a rice α-amylase and cargo proteins to plastids and extracellular compartments of plant cells. *Plant Physiol.* 135: 1367–1377.

Chen, M.H., Liu, L.F., Chen, Y.R., Wu, H.K., and Yu, S.M. (1994). Expression of α-amylase, carbohydrate metabolism, and autophagy in cultured rice cells is coordinately regulated by sugar nutrient. *Plant J.* 6: 625–636.

Chou M-L, Chu C-C, Chen L-J, Akita M, Li H-m. (2006). Stimulation of transit-peptide release and ATP hydrolysis by a cochaperone during protein import into chloroplasts. *J. Cell Biol.* 175:893–900

Gaikwad, A., Tewari, K.K., Kumar, D., Chen, W., and Mukherjee, S.K. (1999). Isolation and characterization of the cDNA encoding a glycosylated accessory protein of pea chloroplast DNA polymerase. *Nucleic Acids Res.* 27: 3120–3129.

Fuji, K., Shimada, T., Takahashi, H., Tamura, K., Koumoto, Y., Utsumi, S., Nishizawa, K., Maruyama, N., and Hara-Nishimura, I. (2007). Arabidopsis vacuolar sorting mutants (green fluorescent seed) can be identified efficiently by secretion of vacuole-targeted green fluorescent protein in their seeds. *Plant Cell* 19: 597–609.

Hayashi, M., Turu, A., Mitsui, T., Takahashi, N., Hanzawa, H., Arata, Y., and Akazawa, T. (1990). Structure and biosynthesis of the xylosecontaining carbohydrate moiety of rice α-amylase. *Eur. J. Biochem.* 191: 287–295.

Hiei, Y., Ohta, S., Komari, T., and Kumashiro, T. (1994). Efficient transformation of rice (Oryza sativa L.) mediated by Agrobacterium and sequence analysis of the boundaries of the T-DNA. *Plant J.* 6: 271–282.

Hood, E.E., Helmer, G.L., Fraley, R.T., and Chilton, M.D. (1986). The hyper-virulence of Agrobacterium tumefaciens A281 is encoded in a region of pTiBo542 outside of T-DNA. *J. Bacteriol.* 168: 1291–1301.

Hummel E, Osterrieder A, Robinson DG, Hawes C, (2010), Inhibition of Golgi function causes plastid starch accumulation. *J. Exp. Bot.*, 61(10):2603-2614

Inoue H, Akita M. (2008). Three sets of translocation intermediates are formed during the early stage ofprotein import into chloroplasts. *J. Biol. Chem.* 283:7491–502

Ishida, H., Yoshimoto, K., Izumi, M., Reisen, D., Yano, Y., Makino, A., Ohsumi, Y., Hanson, M.R., and Mae, T. (2008). Mobilization of Rubisco and stromal-localized fluorescent proteins of chloroplasts to the vacuole by an ATG gene-dependent autophagic process. *Plant Physiol.* 148: 142–155.

Itoh, K., Ozaki, H., Okada, K., Hori, H., Takeda, Y., and Mitsui, T. (2003). Introduction of Wx transgene into rice wx mutants leads to both high- and low-amylose rice. *Plant Cell Physiol.* 44: 473–480.

Jarvis, P. (2008). Targeting of nucleus-encoded proteins to chloroplasts in plants. *New Phytol.* 179: 257–285.

Kim, D.H., Eu, Y.J., Yoo, C.M., Kim, Y.W., Pih, K.T., Jin, J.B., Kim, S.J., Stenmark, H., and Hwang, I. (2001). Trafficking of phosphatidylinositol 3-phosphate from the *trans*-Golgi network to the lumen of the central vacuole in plant cells. *Plant Cell* 13: 287–301.

Kirsch, T., Saalbach, G., Raikhel, N.V., and Beevers, L. (1996). Interaction of a potential vacuolar targeting receptor with aminoand carboxyl-terminal targeting determinants. *Plant Physiol.* 111: 469–474.

Kleffmann, T., Russenberger, D., von Zychlinski, A., Christopher, W., Sjolander, K., Gruissem, W., and Baginsky, S. (2004). The Arabidopsis thaliana chloroplast proteome reveals pathway abundance and novel protein functions. *Curr. Biol.* 14: 354–362.

Klösgen, R.B., and Weil, J.H. (1991). Subcellular location and expression level of a chimeric protein consisting of the maize waxy transit peptide and the beta-glucuronidase of Escherichia coli in transgenic potato plants. *Mol. Gen. Genet.* 225: 297–304.

Kornfeld, R., and Kornfeld, S. (1985). Assembly of asparagine-linked oligosaccharides. *Annu. Rev. Biochem.* 54: 631–664.

Latijnhouwers, M., Hawes, C., Carvalho, C., Oparka, K., Gillingham, A.K., and Boevink, P. (2005). An Arabidopsis GRIP domain protein locates to the *trans*-Golgi and binds the small GTPase ARL1. *Plant J.* 44: 459–470.

Losev, E., Reinke, C.A., Jellen, J., Strongin, D.E., Bevis, B.J., and Glick, B.S. (2006). Golgi maturation visualized in living yeast. *Nature* 441: 1002–1006.

May T. and Soll J. (2000). 14-3-3 proteins form a guidance complex with chloroplast precursor proteins in plants. *Plant Cell* 12:53–63

Mano, S., Nakamori, C., Hayashi, M., Kato, A., Kondo, M., and Nishimura, M. (2002). Distribution and characterization of peroxisomes in Arabidopsis by visualization with GFP: Dynamic morphology and actin-dependent movement. *Plant Cell Physiol.* 43: 331–341.

Matsuoka, K., and Neuhaus, J. (1999). Cis-elements of protein transport to the plant vacuoles. *J. Exp. Bot.* 50: 165–174.

Matsuura-Tokita, K., Takeuchi, M., Ichihara, A., Mikuriya, K., and Nakano, A. (2006). Live imaging of yeast Golgi cisternal maturation. *Nature* 441: 1007–1010.

Mitsui, T., Loboda, T., Kamimura, I., Hori, H., Itoh, K., and Mitsunaga, S. (1999). Sucrose-controlled transport and turnover of α-amylase in rice (Oryza sativa L.) cells. *Plant Cell Physiol.* 40: 884–893.

Mitsui, T., Yamaguchi, J., and Akazawa, T. (1996). Physicochemical and serological characterization of rice α-amylase isoforms and identification of their corresponding genes. *Plant Physiol.* 110: 1395–1404.

Nanjo, Y., Asatsuma, S., Itoh, K., Hori, H., and Mitsui, T. (2004). Proteomic identification of α-amylase isoforms encoded by RAmy3B/3C from germinating rice seeds. *Biosci. Biotechnol. Biochem.* 68: 112–118.

Nanjo, Y., Oka, H., Ikarashi, N., Kaneko, K., Kitajima, A., Mitsui, T., Muñoz, F.J., Rodríguez-López, M., Baroja-Fernández, E., and Pozueta-Romero, J. (2006). Rice plastidial *N*-glycosylated nucleotide pyrophosphatase/phosphodiesterase is transported from the ER Golgi to the chloroplast through the secretory pathway. *Plant Cell* 18: 2582–2592.

Nebenführ, A., Frohlick, J.A., and Staehelin, L.A. (2000). Redistribution of Golgi stacks and other organelles during mitosis and cytokinesis in plant cells. *Plant Physiol.* 124: 135–151.

Nebenführ, A., Gallagher, L.A., Dunahay, T.G., Frohlick, J.A., Mazurkiewicz, A.M., Meehl, J.B., and Staehelin, L.A. (1999). Stop-and-go movements of plant Golgi stacks are mediated by the acto-myosin system. *Plant Physiol.* 121: 1127–1142.

Niwa, Y., Hirano, T., Yoshimoto, K., Shimizu, M., and Kobayashi, H. (1999). Non-invasive quantitative detection and applications of nontoxic, S65T-type green fluorescent protein in living plants. *Plant J.* 18: 455–463.

Palade, G. (1975). Intracellular aspects of the process of protein synthesis. *Science* 189: 347–358.

Qbadou S, Becker T, Mirus O, Tews I, Soll J, Schleiff E. (2006). The molecular chaperone Hsp90 delivers precursor proteins to the chloroplast import receptor Toc64. *EMBO J.* 25:1836–47

Ritzenthaler, C., Nebenfuhr, A., Movafeghi, A., Stussi-Garaud, C., Behnia, L., Pimpl, P., Staehelin, L.A., and Robinson, D.G. (2002). Reevaluation of the effects of Brefeldin A on plant cells using tobacco Bright Yellow 2 cells expressing Golgi-targeted green fluorescent protein and COPI antisera. *Plant Cell* 14: 237–261.

Radhamony, R.N., and Theg, S.M. (2006). Evidence for an ER to Golgi to chloroplast protein transport pathway. *Trends Cell Biol.* 16: 385–387.

Robert, X., Haser, R., Mori, H., Svensson, B., and Aghajari, N. (2005). Oligosaccharide binding to barley α-amylase 1. *J. Biol. Chem.* 280: 32968–32978.

Rothman, J.E., and Wieland, F.T. (1996). Protein sorting by transport vesicles. *Science* 272: 227–234.

Saalbach, G., Jung, R., Kunze, G., Saalbach, I., Adler, K., and Muntz, K. (1991). Different legumin protein domains act as vacuolar targeting signals. *Plant Cell* 3: 695–708.

Søgaard, M., Kadziola, A., Haser, R., and Svensson, B. (1993). Sitedirected mutagenesis of histidine 93, aspartic acid 180, glutamic acid 205, histidine 290, and aspartic acid 291 at the active site and tryptophan 279 at the raw starch binding site in barley α-amylase 1. *J. Biol. Chem.* 268: 22480–22484.

Staehelin, L.A., and Moore, I. (1995). The plant Golgi apparatus: Structure, functional organization and trafficking mechanisms. *Annu. Rev. Plant Physiol. Plant Mol. Biol.* 46: 261–288.

Takeuchi, M., Ueda, T., Sato, K., Abe, H., Nagata, T., and Nakano, A. (2000). A dominant negative mutant of sar1 GTPase inhibits protein transport from the endoplasmic reticulum to the Golgi apparatus in tobacco and Arabidopsis cultured cells. *Plant J.* 23: 517–525.

Takeuchi, M., Ueda, T., Yahara, N., and Nakano, A. (2002). Arf1 GTPase plays roles in the protein traffic between the endoplasmic reticulum and the Golgi apparatus in tobacco and Arabidopsis cultured cells. *Plant J.* 31: 499–515.

Terashima, M., Kubo, A., Suzawa, M., Itoh, Y., and Katoh, S. (1994). The roles of the *N*-linked carbohydrate chain of rice α-amylase in thermostability and enzyme kinetics. *Eur. J. Biochem.* 226: 249–254.

Törmäkangas, K., Hadlington, J.L., Pimpl, P., Hillmer, S., Brandizzi, F., Teeri, T.H., and Denecke, J. (2001). A vacuolar sorting domain may also influence the way in which proteins leave the endoplasmic reticulum. *Plant Cell* 13: 2021–2032.

Toyooka, K., Goto, Y., Asatsuma, S., Koizumi, M., Mitsui, T., and Matsuoka, K. (2009). A mobile secretory vesicle cluster involved in mass transport from the Golgi to plant cell exterior. *Plant Cell* 21: 1212–1229.

Toyooka, K., Moriyasu, Y., Goto, Y., Takeuchi, M., Fukuda, H., and Matsuoka, K. (2006). Protein aggregates are transported to vacuoles by a macroautophagic mechanism in nutrient-starved plant cells. *Autophagy* 2: 96–106.

van Dooren, G.G., Schwartzbach, S.D., Osafune, T., and McFadden, G.I. (2001). Translocation of proteins across the multiple membranes of complex plastids. *Biochim. Biophys. Acta* 1541: 34–53.

von Schaewen, A., and Chrispeels, M.J. (1993). Identification of vacuolar sorting information in phytohemagglutinin, an unprocessed vacuolar protein. *J. Exp. Bot.* 44: 339–342.

Villarejo, A., et al. (2005). Evidence for a protein transported through the secretory pathway en route to the higher plant chloroplast. *Nat. Cell Biol.* 7: 1224–1231.

Vitale, A., and Hinz, G. (2005). Sorting of proteins to storage vacuoles: how many mechanisms? *Trends Plant Sci.* 10: 316–323.

Waegemann K, Soll J. (1996). Phosphorylation of the transit sequence of chloroplast precursor proteins. *J. Biol. Chem.* 271:6545–54

Yu, T.S., et al. (2005). α-Amylase is not required for breakdown of transitory starch in Arabidopsis leaves. *J. Biol. Chem.* 280: 9773–9779.